## Semiclassical Model

High-order harmonic generation was discovered in 1987, although the mechanics was not revealed until 1993. In that year, Corkum and Kulander independently developed a semiclassical model that solved the mystery of the underlying physics of high harmonic generation. This model, for which, the full quantum treatment is provided in full in Chapter 5, laid the theoretical foundation for attosecond optics.

## 4.1 Three-Step Model

In the semiclassical model, an attosecond pulse is generated in three steps within one laser cycle. An artistic presentation of the model is shown in Figure 4.1.

For simplicity, we consider the one-dimensional case and assume that the laser is a monochromatic light, linearly polarized in the x direction. Under these conditions, the laser field at a given spatial point can be expressed as

$$\varepsilon_L(t) = E_L \cos(\omega_0 t), \tag{4.1}$$

which is shown in Figure 4.2. The subscript "0" in  $\omega_0$  specifies that the field oscillates with the fundamental frequency of the laser. We use the cosine form of the field and the initial phase is set to zero. To make the discussion applicable to lasers with a variety of center frequencies, we use normalized quantities: time is normalized to the laser period,  $T_0$ , and the angular frequency to  $\omega_0 = 2\pi/T_0$  For reference, a Ti:Sapphire laser has a period of  $T_0 = 2.67$  fs.

Suppose an atom is located at x = 0. In the first step, the potential well of the atom where the electron is trapped is turning into a potential barrier by the laser field. The bound electron is freed (ionized) by tunneling through the barrier. This step is a quantum process, which is discussed in detail later in this chapter. We assume that the ionization is instantaneous, which means that the ionization rate at a given time only depends on the laser-field strength at that time. When the electron is freed, its initial position is also at x = 0. We further assume that the initial velocity of the electron is  $v_0 = 0$ .

In the second step, we assume the freed electron moves in the laser field and we neglect the Coulomb field of the atom. The electron is treated classically, which means that the equation of motion of a free electron is



**Figure 4.1** The three-step model. (Reprinted from P.B. Corkum and Z. Chang, *Opt. Photon. News*, 19, 24, 2008.)

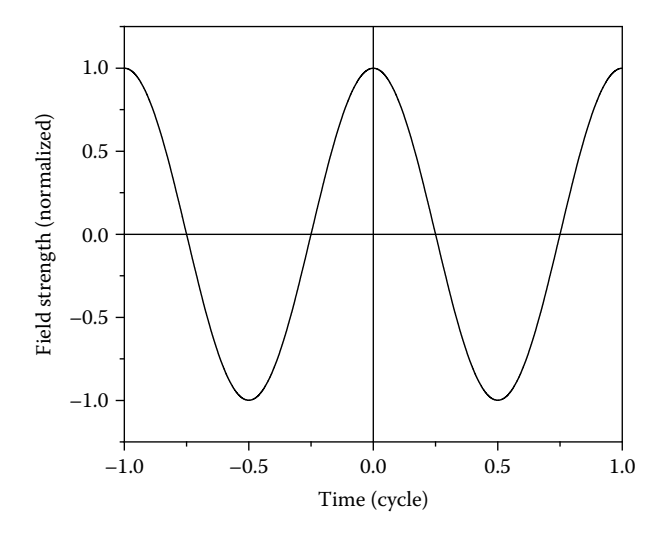


Figure 4.2 The laser field in the three-step model.

$$\frac{d^2x}{dt^2} = -\frac{e}{m_e}\varepsilon_L(t) = -\frac{e}{m_e}E_L\cos(\omega_0 t),\tag{4.2}$$

where -e and  $m_e$  are the charge and mass of the electron, respectively. Assuming an electron is freed at time t', the solution of the equation is

$$v(t) = -\frac{eE_L}{m_e\omega_0} \left[ \sin\left(\omega_0 t\right) - \sin\left(\omega_0 t'\right) \right],\tag{4.3}$$

$$x(t) = \frac{eE_L}{m_e \omega_0^2} \{ [\cos(\omega_0 t) - \cos(\omega_0 t')] + \omega_0 \sin(\omega_0 t')(t - t') \},$$
(4.4)

where v is the velocity of the electron.

We define  $x_0 = 2eE_L/m_e\omega_0^2$ . Equation 4.4 can be normalized to

$$\frac{x(t)}{x_0} = \frac{1}{2} \left[ \cos(\omega_0 t) - \cos(\omega_0 t') + \sin(\omega_0 t') \omega_0 (t - t') \right], \tag{4.5}$$

The normalized electron trajectory for an electron released at  $\omega_0 t' = 0$  is shown in Figure 4.3. The figure shows that  $x_0$  is the maximum displacement of the electron ionized at t' = 0. The typical Ti:Sapphire laser intensity for attosecond pulse generation is  $E_L = 5 \times 10^{14} \text{ W/cm}^2$ , which gives  $x_0 = 1.95 \text{ nm}$ . This electron returns to the parent ion one cycle later. Electrons ionized at other times take different trajectories; some of them can return, and some drift away.

In the third step, the electron recombines with the parent ion at x = 0 and emits a photon. The emitted photon energy is

$$\hbar\omega_X(t) = I_p + \frac{1}{2}mv^2(t) = I_p + 2U_p[\sin(\omega_0 t) - \sin(\omega_0 t')]^2,$$
 (4.6)

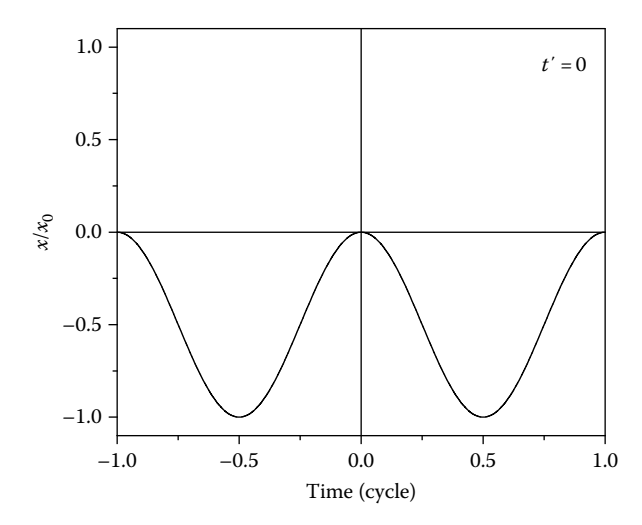


Figure 4.3 The trajectory of an electron in the laser field.

where  $I_p$  is the ionization potential of the atom and the ponderomotive energy,  $U_p$ , is given by

$$U_p = \frac{(eE_0)^2}{4m\omega_0^2}. (4.7)$$

The electron ionized at t'=0 returns with zero kinetic energy, and the corresponding photon energy is equal to  $I_p$ . This step is also a quantum process, which is discussed in the next chapter.

Several important features of high harmonic generation and attosecond pulses can be understood from the classical treatment of the electron in the second step and by using the energy conservation law. A few of these features in particular are the cutoff photon energy of the attosecond/high harmonic spectrum and the chirp of the attosecond pulses. Similar analyses can be applied to understand the energy spectra of the electrons freed by the above-threshold ionization and by the tunneling ionization.

#### 4.1.1 Recombination Time

When the electron returns to the parent ion at time t, its position x(t) = 0. This is the time that the recombination occurs. The time t can be found by solving the equation

$$x(t) \propto \cos(\omega_0 t) - \cos(\omega_0 t') + \omega_0 \sin(\omega_0 t')(t - t') = 0. \tag{4.8}$$

#### 4.1.1.1 Graphic Solutions and Kramers-Henneberger Frame

Equation 4.8 has no analytical solutions, but the solutions can be found out graphically, as shown in Figure 4.4. The equation can be rewritten as

$$\cos(\omega_0 t) - \cos(\omega_0 t') = \frac{d}{d(\omega_0 t)} \cos(\omega_0 t) \Big|_{t'} (\omega_0 t - \omega_0 t'). \tag{4.9}$$

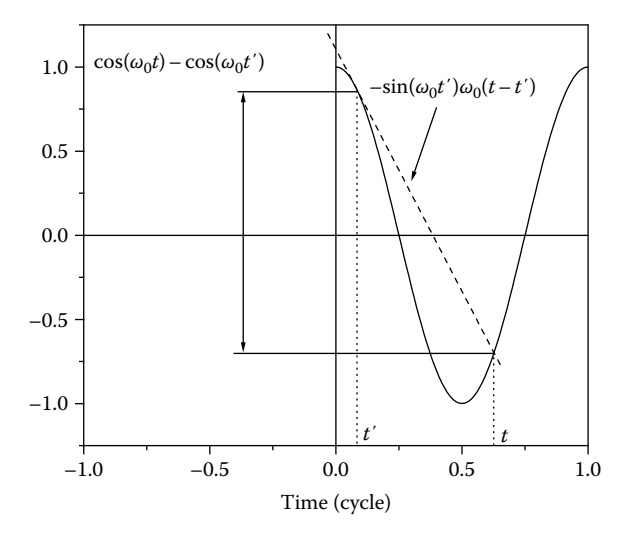
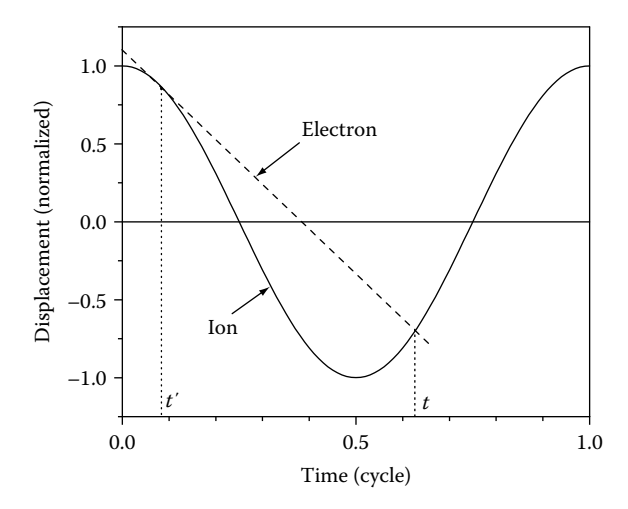


Figure 4.4 Graphic solution of the equation of motion.



**Figure 4.5** The normalized trajectories of the ion and electron in the Kramers–Henneberger frame.

First, we plot  $\cos(\omega_0 t)$ , then draw a straight line starting at  $\cos(\omega_0 t')$  that is tangent to the  $\cos(\omega_0 t)$  curve, i.e., the slope is  $\frac{d}{d(\omega_0 t)}\cos(\omega_0 t)\Big|_{t'} = -\sin(\omega_0 t')$ . If the straight line crosses the  $\cos(\omega_0 t)$  curve at a later time t, then t is the recombination time for the electron releasing time t'.

The graphical approach corresponds to a reference frame called Kramers–Henneberger frame, as illustrated in Figure 4.5. In this reference frame, the parent ion is moving periodically such that its displacement follows  $\cos(\omega_0 t)$  and the electron motion is a linear displacement. The slope of the line is  $-\sin(\omega_0 t')$ , just like in the case in Figure 4.4. In other words, the electron and ion motion in this frame provides physical meanings to the graphic method.

It can be seen that electrons emitted at time  $\omega_0 t'=0$  return one cycle  $(T_0)$  later  $\omega_0 t=2\pi$ .  $t-t'=T_0$  is the maximum roundtrip time that electron can have in the laser field. For  $\omega_0 t'=\pi/2$ ,  $\omega_0 t=\pi/2$ , i.e., electron never leaves the parent ion. All electrons ionized in the time range  $\omega_0 t'=0$  to  $\omega_0 t'=\pi/2$  can return to the parent ion. However, if an electron is released during  $\omega_0 t'=\pi/2$  to  $\omega_0 t'=\pi$ , it will never return to the parent ion. Since the laser field is sinusoidal, electrons ionized during  $\omega_0 t'=\pi/2$  to  $\omega_0 t'=(3/2)\pi$  will return, but from an opposite direction as compared to an electron ionized during  $\omega_0 t'=0$  to  $\omega_0 t'=\pi/2$ .

#### 4.1.1.2 Numerical Solutions and Fitting Functions

Equation 4.8 can also be solved numerically. The solution is shown in Figure 4.6.

The solution can be well fitted with a simple analytical function

$$\frac{t}{T_0} = \frac{1}{4} - \frac{3}{2\pi} \sin^{-1}\left(4\frac{t'}{T_0} - 1\right). \tag{4.10}$$

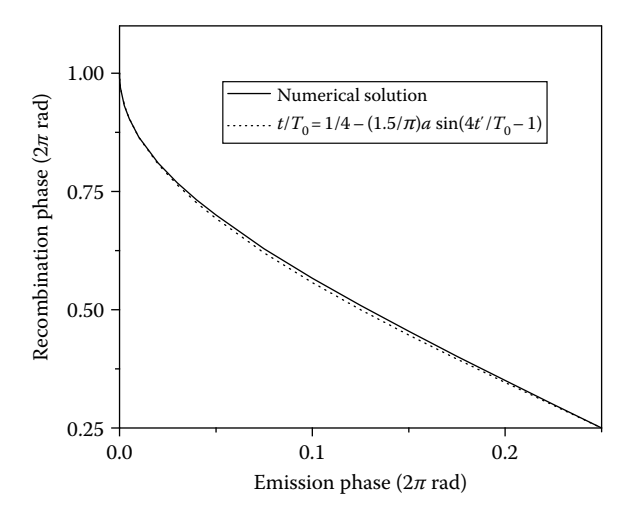


**Figure 4.6** Dependence of the recombination time on the releasing time.

Or in terms of phases

$$\omega_0 t = \frac{\pi}{2} - 3\sin^{-1}\left(\frac{2}{\pi}\omega_0 t' - 1\right). \tag{4.11}$$

The fitting function is also shown in Figure 4.6 for comparison.

The fact that the returning time spans over 0.75 laser cycle suggests that the emitted electromagnetic pulse may last for  $0.75T_0$  time period, which is 2 fs for Ti:Sapphire. The FWHM could be less than  $0.75T_0 \times 0.5 = 1$  fs. This is the origin of the attosecond pulse generation.

## 4.1.2 Return Energy

The kinetic energy of the returning electron normalized by the ponderomotive energy is

$$\frac{K}{U_p} = 2\left[\sin\left(\omega_0 t\right) - \sin\left(\omega_0 t'\right)\right]^2. \tag{4.12}$$

Inserting Equation 4.11 into Equation 4.12, we have

$$\frac{K(\omega_0 t')}{U_p} = 2\left[\cos\left(3\sin^{-1}\left(\frac{2}{\pi}\omega_0 t' - 1\right)\right) - \sin\left(\omega_0 t'\right)\right]^2. \tag{4.13}$$

The dependence of the kinetic energy on the emission time calculated using Equations 4.12 and 4.13 is shown in Figure 4.7, which was obtained by inserting the t and its corresponding t' in Figure 4.6 to Equation 4.10.

The maximum kinetic energy is

$$K_{\text{max}} \approx 3.17 U_p, \tag{4.14}$$

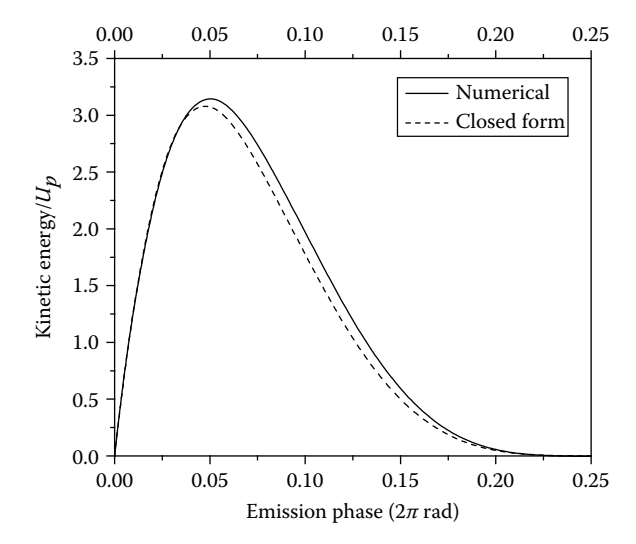


Figure 4.7 The kinetic energy of the returned electron.

which is carried by the electron released at  $\omega_0 t' = 0.05 \times 2\pi$  rad and returns at  $\omega_0 t = 0.7 \times 2\pi$ . Thus, the maximum photon energy is

$$\hbar\omega_{X, \max} = I_p + 3.17U_p.$$
 (4.15)

With this very important prediction of the semiclassical model, we can calculate the cutoff order of the high harmonic spectrum and the upper limit of the attosecond spectrum.

The ponderomotive energy can also be expressed as

$$U_p[eV] = 9.33 \times 10^{-14} I_L \lambda_0^2,$$
 (4.16)

where  $I_L$  is the intensity of the laser in W/cm<sup>2</sup>. The unit of the laser wavelength is  $\mu$ m. Equations 4.15 and 4.16 suggest that the cutoff photon energy can be extended by using a long wavelength laser. This prediction has been confirmed by experiments.

For example, for argon atoms,  $I_p = 15.78$  eV. The highest intensity of femtosecond lasers they can withstand can reach  $3 \times 10^{14}$  W/cm<sup>2</sup>. The corresponding ponderomotive energy is  $\sim 18$  eV while the maximum photon energy can reach  $\sim 72$  eV! This puts the radiation in the XUV range.

## 4.1.3 Long and Short Trajectories

Figure 4.7 shows that one electron released at time  $t' < 0.05T_0$  can have the same kinetic energy as another one freed at time  $t' > 0.05T_0$ . An electron released earlier in time will return later in time, as shown in Figure 4.6, thus giving it a longer round trip time. It is for this reason that the trajectory of the electron released before  $0.05T_0$  is called the "long-trajectory" electron while those released after  $0.05T_0$  are called the "short-trajectory" electrons.

Experimentally, it is possible to suppress the long trajectory by phase matching and spatial filtering, which is discussed in Chapter 5. In that case, only the electrons in the short trajectory can arrive at the detector. The return time of the short trajectory extends from  $t = 0.25T_0$  to  $0.7T_0$ , which is 1.2 fs, or a possible 600 as at FWHM. Therefore, it is possible to generate attosecond pulses by using the short trajectory. To estimate the XUV pulse width more accurately, we need to know the dependence of the ionization rate on the electron recombination time, which is discussed later in the chapter.

## 4.1.4 Chirp of Attosecond Pulses

Since the kinetic energy of the electron depends on the return time, the photon energy also changes with time, which is the origin of the chirp of attosecond pulses. The degree of the chirp,  $d\omega_x(t)/dt \propto dK(t)/dt$ , can be obtained from the equation

$$\frac{\hbar\omega_X(t) - I_p}{U_p} = \frac{K(t)}{U_p} = 2\left[\sin\left(\omega_0 t\right) - \sin\left(\omega_0 t'\right)\right]^2,\tag{4.17}$$

Equation 4.11 can be rewritten as

$$\sin(\omega_0 t') = \cos\left[\frac{\pi}{2}\sin\left(\frac{1}{3}\omega_0 t - \frac{\pi}{6}\right)\right]. \tag{4.18}$$

Inserting Equation 4.18 into Equation 4.17 gives

$$\frac{K(t)}{U_p} = 2\left\{\sin\left(\omega_0 t\right) - \cos\left[\frac{\pi}{2}\sin\left(\frac{1}{3}\omega_0 t - \frac{\pi}{6}\right)\right]\right\}^2. \tag{4.19}$$

which is shown in Figure 4.8.

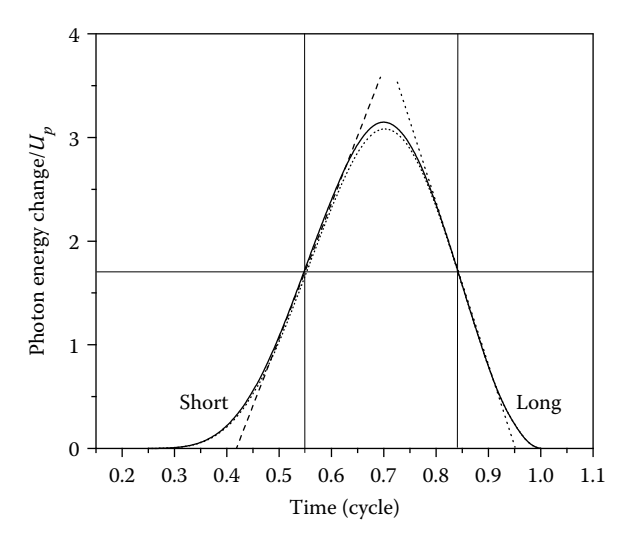


Figure 4.8 Chirp of the attosecond radiation.

Interestingly, the short trajectory is positively chirped, dK(t)/dt > 0, whereas the long trajectory is negatively chirped, dK(t)/dt < 0. The chirp, i.e., the slope of the curve in Figure 4.8, is almost linear over a broad photon energy range. The values of the chirp can be terminated by the slopes at  $\hbar\omega_X(t) - I_p/U_p = 5.5$ , which corresponds to  $t = 0.55T_0$  for the short trajectory and  $t = 0.85T_0$  for the long trajectory.

The slopes can be determined by

$$\frac{1}{U_p} \frac{d}{dt} (\hbar \omega_X) = 4 \left[ \sin \left( \omega_0 t \right) - \sin \left( \omega_0 t' \right) \right] \\
\times \left[ \cos \left( \omega_0 t \right) - \cos \left( \omega_0 t' \right) \frac{dt'}{dt} \right] \frac{2\pi}{T_0}.$$
(4.20)

Equation 4.20 can be rewritten in a dimensionless format as

$$\frac{T_0}{U_p} \frac{d}{dt} (\hbar \omega_X) = 8\pi \left[ \sin(\omega_0 t) - \sin(\omega_0 t') \right] \times \left[ \cos(\omega_0 t) - \cos(\omega_0 t') \frac{dt'}{dt} \right].$$
(4.21)

Next, we can introduce an auxiliary function that corresponds to electron displacement

$$x(t, t') = \cos(\omega_0 t) - \cos(\omega_0 t') + \sin(\omega_0 t')(\omega_0 t - \omega_0 t'). \tag{4.22}$$

Using the theory of partial derivatives,

$$\frac{dt'}{dt} = \left(\frac{\partial t'}{\partial t}\right)_{x} = \frac{-\left(\frac{\partial x}{\partial t}\right)_{t'}}{\left(\frac{\partial x}{\partial t'}\right)_{t}} = \frac{\sin(\omega_{0}t) - \sin(\omega_{0}t')}{\cos(\omega_{0}t')(\omega_{0}t - \omega_{0}t')}.$$
(4.23)

If Equation 4.23 is inserted into Equation 4.21, we have

$$\frac{T_0}{U_p} \frac{d}{dt} (\hbar \omega_X) = 8\pi \left[ \sin \left( \omega_0 t \right) - \sin \left( \omega_0 t' \right) \right] \\
\times \left[ \cos \left( \omega_0 t \right) - \frac{\sin \left( \omega_0 t \right) - \sin \left( \omega_0 t' \right)}{\omega_0 t - \omega_0 t'} \right].$$
(4.24)

The chirp is defined as

$$C = \frac{dt}{d(\hbar\omega_X)},\tag{4.25}$$

Finally,

$$C(t,t') = -\frac{T_0}{U_p}$$

$$\times \frac{\omega_0(t-t')}{8\pi[\sin(\omega_0 t) - \sin(\omega_0 t')][\sin(\omega_0 t) - \sin(\omega_0 t') - \cos(\omega_0 t)\omega_0(t-t')]},$$
(4.26)

An explicit expression for the chirp as a function of return time can be obtained by using Equation 4.18, which gives

$$C(t) = \frac{T_0}{U_p} \times \frac{1}{4\pi K(t) \left\{ \cos\left(\omega_0 t\right) + \frac{\pi}{6} \cos\left(\frac{1}{3}\omega_0 t - \frac{\pi}{6}\right) \sin\left[\frac{\pi}{2} \sin\left(\frac{1}{3}\omega_0 t - \frac{\pi}{6}\right)\right] \right\}}.$$
(4.27)

#### 4.1.4.1 Short Trajectory

The releasing time corresponding to  $t = 0.55T_0$  is  $t' = 0.107T_0$ . Inserting them into Equation 4.24, we get

$$\frac{T_0}{U_p}\frac{d}{dt}(\hbar\omega_X) = 14.43. \tag{4.28}$$

Thus, the chirp is

$$C = \frac{dt}{d(\hbar\omega_X)} = 0.069 \frac{T_0}{U_p}.$$
 (4.29)

To better understand the application of this concept, we can use an example for a Ti:Sapphire laser with a period of  $T_0 = 2.67$  fs. When the intensity is  $3 \times 10^{14}$  W/cm<sup>2</sup>, the chirp is C = 10 as/eV. The chirp is therefore inversely proportional to the laser intensity, thus C = 30 as/eV at  $1 \times 10^{14}$  W/cm<sup>2</sup>.

In laser optics, the unit of the chirp is as<sup>2</sup>, which can be calculated using the following conversion:

$$C[as^2] = \frac{c[as/eV]}{1.516} 10^3.$$
 (4.30)

A typical chirp is 10 as/eV, or  $6.6 \times 10^3$  as<sup>2</sup>.

Equation 4.30 can also be expressed in terms of laser intensity and the center wavelength. Since  $T_0 = \lambda_0/c$ , we have

$$C[as/eV] = 24.7 \times 10^{14} \frac{1}{I_0 \lambda_0},$$
 (4.31)

where  $I_0$  is in W/cm<sup>2</sup> and the unit of the laser wavelength is expressed in  $\mu$ m. It is clear that the chirp can be reduced by either increasing the laser intensity or using a long wavelength laser. The chirp can be compensated by materials that have negative group velocity dispersion, as is discussed in Chapter 1.

#### 4.1.4.2 Long Trajectory

The releasing time corresponding to  $t = 0.85T_0$  is  $t' = 0.0123T_0$ . The chirp then becomes

$$C = -0.059 \frac{T_0}{U_n}. (4.32)$$

The chirp is negative, meaning that the high-energy photons are emitted before the low-energy ones. The magnitude of the chirp is a little less than that of the short trajectory.

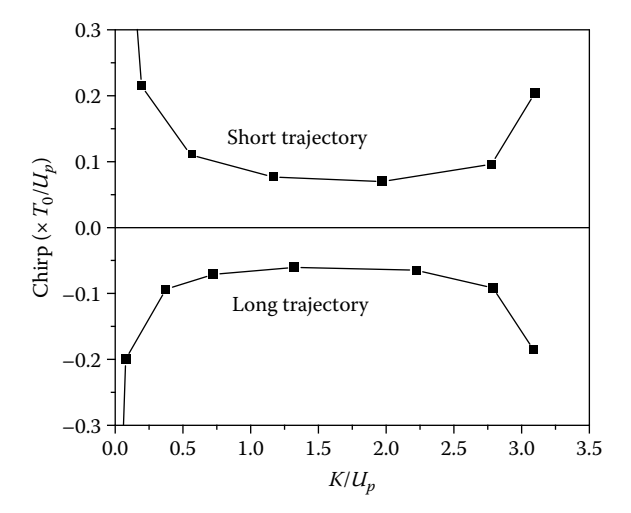


**Figure 4.9** The chirp in unit of  $T_0/U_D$  as function of  $K/U_D$ .

#### 4.1.4.3 The General Case

Equations 4.28 through 4.32 are used in the spectral region where the chirp is close to linear. In general, the attosecond chirp can be obtained using Equation 4.26. The dependence of the chirp on the kinetic energy is shown in Figure 4.9. It is worthwhile to mention that this dependence is not a function of the ionization potential of the atom.

### 4.1.4.4 High-Order Chirp

The graph in Figure 4.9 shows that the chirp is not a constant near the cutoff of the spectrum. This is partly due to the fact that in the cutoff region the third-order phase and other high-order phases start to show up.

The third-order chirp, TOC, is defined as

$$TOC = \frac{d}{d\omega_x} \left( \frac{dt}{d\omega_x} \right), \tag{4.33}$$

which is the slope of the curve in Figure 4.9.

# 4.2 Tunneling Ionization and Multiphoton Ionization

In the three-step model of attosecond pulse generation, the first step is the ionization of an atom by the laser field. The ionization rate is needed to determine the temporal profile of the electron pulse returning to the parent ion, which is related to the attosecond pulse duration. Simple analytic solutions of the ionization rate have been found under various approximations. The rate expressions have been frequently used in order to avoid solving Schrödinger Equation numerically.

## 4.2.1 The Keldysh Theory

Rare gases are commonly used to generate attosecond pulses because they can withstand high laser intensity. Their ionization potentials are in the range of 12.1–24.5 eV, which is much larger than the photon energy of the NIR laser (<2 eV). In the 1960s, Keldysh developed a very important theory for one-electron atom photoionization by strong lasers when the laser photon energy is much smaller than the ionization potential. Using a first-order perturbation theory, he derived the photoionization formula for the direct transition between the electronic ground state and the Volkov continuum state, which includes oscillatory motion of the free electron in the time-dependent linearly polarized electric field. The intermediate resonance states were not taken into consideration by this theory. Neglecting the resonance bound states as well as the effects Coulomb potential on the continuum states is named strong field approximation.

Subsequently, Faisal considered an *S*-matrix theory in which the initial bound state is dressed by the laser field and the final ionization state is taken to be noninteracting. Later, Reiss established a rigorous basis for an extended version of the Keldysh theory in which systematic higher-order corrections can be applied to the Keldysh term. Combined, these are well known as the so-called Keldysh–Faisal–Reiss theory.

#### 4.2.1.1 Volkov States

The Schrodinger Equation for an atom in a laser field is given by

$$i\hbar \frac{d}{dt}\Psi(\vec{r},t) = [H_0 + H_I]\Psi(\vec{r},t), \tag{4.34}$$

where

 $H_0$  is the contribution to the total Hamiltonian from the atom  $H_I(t)$  is from the laser field

Far from the atom,  $H_0 = 0$ , the effects of the Coulomb field of the atom can be ignored. The equation is simplified to

$$i\hbar \frac{d}{dt}\psi(\vec{r},t) = H_I(t)\psi(\vec{r},t). \tag{4.35}$$

We use  $\vec{A}$  to denote the vector potential of the electromagnetic field, and use  $\phi$  to denote the scalar potential. In classic mechanics, the Hamiltonian of an electron in the light field is

$$H_{c} = \frac{1}{2m_{e}} \left( \vec{p} + \frac{e}{c} \vec{A} \right)^{2} - e\phi$$

$$= \frac{1}{2m_{e}} p^{2} + \frac{e}{2m_{e}c} \left( \vec{A} \cdot \vec{p} + \vec{p} \cdot \vec{A} \right) + \frac{e^{2}}{2m_{e}c^{2}} A^{2} - e\phi, \qquad (4.36)$$

where  $\vec{p}$  is the canonical momentum. In quantum mechanics, the canonical momentum is replaced by the momentum operator expressed by

$$H_I = \frac{1}{2m_e} \left( \hat{p} + \frac{e}{c} \vec{A} \right)^2 - e\phi,$$
 (4.37)

where  $\hat{p} = -i\hbar\nabla$  is the canonical momentum operator. Apparently

$$H_I = \frac{1}{2m_e}\hat{p}^2 + \frac{e}{2m_ec}(\vec{A} \cdot \hat{p} + \hat{p} \cdot \vec{A}) + \frac{e^2}{2m_ec^2}A^2 - e\phi, \tag{4.38}$$

In general, the  $\vec{A}$  and  $\hat{p}$  are not commutable,  $\hat{p} \cdot \vec{A} - \vec{A} \cdot \hat{p} = -i\hbar \ \nabla \cdot \vec{A}$ . In the Coulomb gauge,  $\nabla \cdot \vec{A} = 0$ ,  $\hat{p} \cdot \vec{A} = \vec{A} \cdot \hat{p}$ .

Since the Coulomb potential is ignored and there is no other static field, thus  $\phi = 0$ . Therefore,

$$H_I = \frac{1}{2m_e}\hat{p}^2 + \frac{e}{m_e c}\vec{A} \cdot \hat{p} + \frac{e^2}{2m_e c^2}A^2. \tag{4.39}$$

Assuming the laser is a monochromatic plane wave that is linearly polarized along the direction defined by the unit vector  $\vec{\varepsilon}$ , the vector potential becomes

$$\vec{A}(t) = -\vec{\varepsilon}A_0 \sin(\omega t), \tag{4.40}$$

and the corresponding electric field is

$$\vec{\varepsilon}(t) = \vec{\varepsilon} F \cos(\omega t). \tag{4.41}$$

Here, F is the amplitude maximum of the incident linearly polarized electric field.

The solutions are eigenstates of the canonical momentum with eigenvalue  $\vec{p} = \vec{p}_m - \frac{e}{c}\vec{A}(t)$ , which is equal to the average drift momentum of the corresponding classical electron. Here  $\vec{p}_m$  is the mechanical momentum of the electron. The solution can be expressed as

$$\psi_{V}(\vec{r},t) = e^{i\frac{1}{\hbar} \left[ \left[ \vec{p}_{m} - \frac{\epsilon}{c} \vec{A}(t) \right] \cdot \vec{r} - \frac{p_{m}^{2}}{2m_{e}} \int_{0}^{t} dt' \left[ \vec{p}_{m} - \frac{\epsilon}{c} \vec{A}(t') \right]^{2} \right]}. \tag{4.42}$$

Using Equation 4.40, we get

$$\psi_{V}(\vec{r},t) = e^{i\frac{1}{\hbar} \left[ \vec{p}_{m} \cdot \vec{r} - \frac{p_{m}^{2}}{2m_{e}t} - U_{p}t \right]} \sum_{n=-\infty}^{\infty} \sum_{m=-\infty}^{\infty} J_{m} \left( \frac{e^{2} A_{0}^{2}}{8\hbar \omega m_{e}c^{2}} \right)$$

$$\times J_{n-2m} \left( |\vec{\varepsilon} \cdot \vec{p}_{m}| \frac{eA_{0}}{\hbar \omega m_{e}c} \right) e^{in\omega t}. \tag{4.43}$$

The  $J_m$  are mth order Bessel functions of the first kind and the eigenstates are called Volkov states which are plane electron waves,  $e^{i(1/\hbar)[\vec{p}_m \cdot \vec{r} - (p_m^2/2m_e)t - U_p t]}$ , with many discrete frequency components  $e^{in\omega t}$ . The spacing between the electron frequency comb is the laser frequency  $\omega$  while the Bessel functions determine the amplitude of each component. Since  $n = -\infty, \ldots, \infty$ , the negative frequency space is also covered.

#### 4.2.1.2 Fermi's Golden Rule and Photoionization Rate

Fermi's golden rule is a way to calculate the transition rate (probability of transition per unit time) from one energy eigenstate of a quantum system into a continuum of energy eigenstates, due to a perturbation  $H_I$ . It is valid when the initial state has not been significantly depleted by scattering into the final states. We consider an atom to begin in an eigenstate  $\Psi_i$  of a given Hamiltonian  $H_0$ . Consider the situation where  $A^2 \ll e/m_e c \vec{A} \cdot \hat{p}$ ,

the transition rate (transition probability per unit time) from an initial state  $\Psi_i$  to a final state  $\Psi_f$  is given, to first order approximation in the perturbation, by

$$w \propto \frac{2\pi}{\hbar} \left| \left\langle \Psi_f | H_I | \Psi_i \right\rangle \right|^2 \propto \left\langle \Psi_f | \vec{A} \cdot \vec{p} | \Psi_i \right\rangle. \tag{4.44}$$

From the Quantum Mechanic relations, we have

$$\left\langle \Psi_f | \vec{A} \cdot \vec{p} | \Psi_i \right\rangle \propto \left\langle \Psi_f | \vec{A} \cdot \nabla V(\vec{r}) | \Psi_i \right\rangle \propto \left\langle \Psi_f | \vec{A} \cdot \vec{r} | \Psi_i \right\rangle$$

$$\propto \left\langle \Psi_f | \vec{\epsilon}(t) \cdot \vec{r} | \Psi_i \right\rangle. \tag{4.45}$$

Quantitatively, the rate of photoionization,

$$w = \frac{1}{(2\pi\hbar)^3} \int d^3v \frac{d}{dT} |c_{\vec{v}}(T)|^2 |_{T \to \infty},$$
 (4.46a)

where  $\vec{v}$  denotes the momentum of the freely ionizing electron

$$c_{\vec{v}}(T) = \frac{i}{\hbar} \int_{0}^{T} dt \left\langle \psi_{\vec{v}}(\vec{r}, t) | e\vec{r} \cdot \vec{\varepsilon} F \cos(\omega t) | \psi_{g}(\vec{r}) e^{-\frac{i}{\hbar} E_{g} t} \right\rangle. \tag{4.46b}$$

The wave function  $\psi_g(\vec{r})$  represents the initial electron ground state with binding energy  $-E_g$ , while  $\psi_{\vec{v}}(\vec{r}, t)$  is the final continuum state. In the Keldysh theory,  $\psi_{\vec{v}}(\vec{r}, t) = \psi_V(\vec{r}, t)$ .

#### 4.2.1.3 Keldysh Parameter

Keldysh introduced a dimensionless parameter to categorize different ionization mechanisms. In atomic units, the Keldysh parameter is expressed as

$$\gamma = \frac{\omega}{F} \sqrt{2I_p} = \sqrt{\frac{I_p}{2U_p}},\tag{4.47}$$

where

 $I_p = -E_g$  is the ionization potential of an atom

 $\omega$  is the laser frequency

F is the laser field strength

The ponderomotive potential

$$U_p = \frac{F^2}{4\omega^2} \tag{4.48}$$

is the cycle average kinetic energy of an electron in the laser field. The  $\gamma$  parameter measures the ratio between the tunneling time  $t_{tu}$ , i.e., the time needed for an electron to cross the Coulomb barrier, and the time during which the same barrier is lowered by the laser field,

$$\gamma = \frac{2\pi}{T_0} \frac{\sqrt{2I_p}}{F} = \frac{t_{tu}}{T_0}.$$
 (4.49)

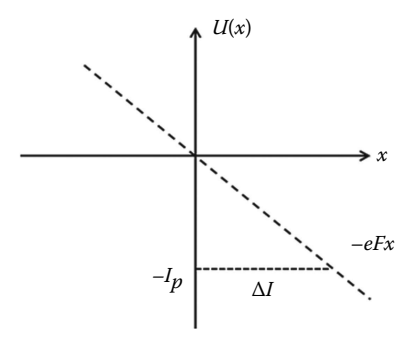


Figure 4.10 The potential barrier formed by the laser field.

In estimating the tunneling time, we assume that the electron velocity inside the barrier is the same as that in the ground state. Under this assumption, the tunneling time becomes

$$t_{tu} = \frac{\Delta l}{v_{or}},\tag{4.50}$$

where

 $\Delta l$  is the width of the barrier

 $v_{gr}$  is the velocity of the electron in the ground state

As shown in Figure 4.10, the barrier width can then be given as

$$\Delta l = \frac{I_p}{F}.\tag{4.51}$$

Since

$$\frac{1}{2}m_e v_{gr}^2 = I_p, (4.52)$$

the electron velocity in atomic unit is

$$v_{gr} = \sqrt{2I_p}. (4.53)$$

Thus,

$$t_{tu} = \frac{1}{2} \frac{\sqrt{2I_p}}{F}.$$
 (4.54)

The Keldysh parameter is defined as

$$\gamma = \frac{t_{tu}}{T_0/2} = \frac{1}{T_0} \frac{\sqrt{2I_p}}{F}.$$
 (4.55)

In an elliptically polarized field with ellipticity,  $\xi$ , the ponderomotive potential is

$$U_p = \frac{e^2 F^2}{4m_e \omega^2} (1 + \xi^2) = \frac{2\pi e^2}{c\omega^2} I. \tag{4.56}$$

Multiphoton ionization of atoms in a laser field occurs when  $\gamma \gg 1$ . In this case, electrons are pulled out of the atom by absorption of several photons.

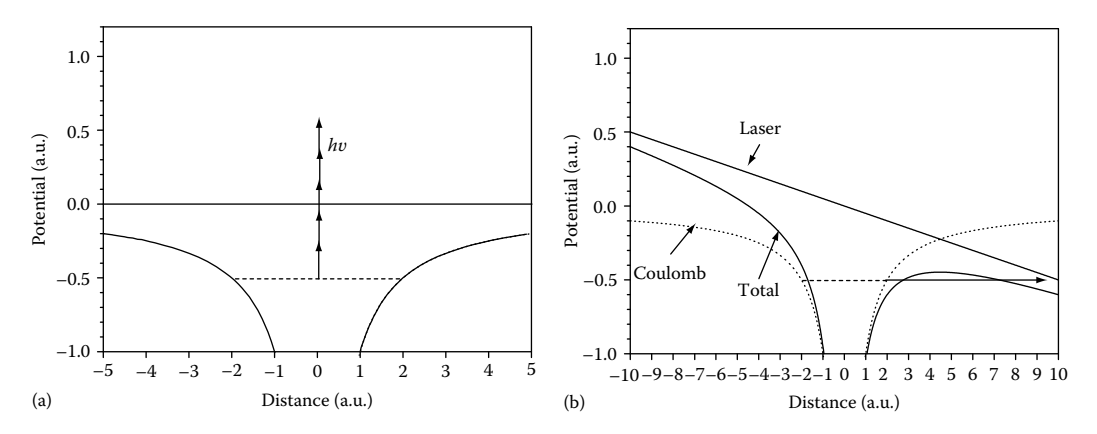


Figure 4.11 (a) Multiphoton ionization. (b) Tunneling ionization.

Tunneling ionization happens when  $\gamma \ll 1$ , where the electron leaves the atomic core by passing through the Coulomb barrier lowered by the laser field. The ionization rate can be calculated by the Perelomov, Popov, and Terent'ev (PPT) model for both types of ionization. The rate can also be calculated by a simpler Ammosov–Delone–Krainov (ADK) Equation in the tunneling regime, given that the rates from the two models are identical for  $\gamma \ll 1$ . The multiphoton ionization and the tunneling ionization process are shown in Figure 4.11.

#### 4.2.2 PPT Model

PPT obtained a formula for the actual three-dimensional atoms in the short-range potentials. Their three-dimensional photoionization rate formulas are applicable for hydrogen atoms with arbitrary initial ground states of orbital angular momentum l and magnetic quantum number m. The theory was extended to other types of atoms and ions by the ADK Theory.

A neutral atom A can be ionized by absorbing q photons, leaving an ion with change Z. The process can be described by  $A+q\omega=A^{+Z}+Ze$ . For single ionization, Z=1. The PPT model was derived for a short-range potential and includes the effect of the long-range Coulomb interaction through the first-order correction in the quasiclassical action, which does not consider any discrete binding states other than the ground state.

In atomic units, the PPT model gives the following total rate of ionization:

$$w_{PPT}(F, \boldsymbol{\omega}) = \sum_{q \ge q_{thr}}^{\infty} w_q(F, \boldsymbol{\omega}), \tag{4.57}$$

where  $q_{thr} = \lceil (I_p + U_p)/\omega \rceil$  is the minimum number of photon required to ionize an electron through the multiphoton process, or, the ionization threshold.  $I_p + U_p$  is the effective ionization potential considering the AC Stark shift and  $\lceil x \rceil$  denotes the ceiling function.

We can assume that the electron is in the state, n, l, m, before the field arrives. Here, n is the principal quantum number, l is the orbital quantum

number, and m is the magnetic quantum number, respectively. In atomic unit, the rate of ionization by absorbing q photons is

$$w_{q}(F,\omega) = A_{q}(\omega,\gamma) |C_{n^{*}l^{*}}|^{2} G_{lm} I_{p} \left(\frac{2F_{o}}{F}\right)^{2n^{*}} \times \left(\frac{2F_{o}}{F} \frac{1}{\sqrt{1+\gamma^{2}}}\right)^{-|m|-1} \frac{4}{\sqrt{3\pi}} \frac{1}{|m|!} \frac{\gamma^{2}}{1+\gamma^{2}} e^{-\frac{2F_{o}}{3F}g(\gamma)}, \quad (4.58)$$

where

$$A_q(\omega, \gamma) = e^{-\alpha(q-\nu)} w_m \left[ \sqrt{\beta(q-\nu)} \right], \tag{4.59}$$

$$v = \frac{I_p}{\omega} \left( 1 + \frac{1}{2\gamma^2} \right) = \frac{I_p + U_p}{\omega},\tag{4.60}$$

$$\alpha(\gamma) = 2 \left[ \sinh^{-1} \gamma - \frac{\gamma}{\sqrt{1 + \gamma^2}} \right], \tag{4.61}$$

$$\beta(\gamma) = \frac{2\gamma}{\sqrt{1+\gamma^2}},\tag{4.62}$$

$$w_m(x) = \frac{x^{2|m|+1}}{2} \int_0^1 \frac{e^{-x^2 t} t^{|m|}}{\sqrt{1-t}} dt.$$
 (4.63)

We can also write the rate as

$$w_{PPT}(F,\omega) = |C_{n^*l^*}|^2 G_{lm} I_p \left(\frac{2F_0}{F}\right)^{2n^* - |m| - 1} \left(\frac{1}{\sqrt{1 + \gamma^2}}\right)^{-|m| - 1}$$

$$\times \frac{4}{\sqrt{3\pi}} \frac{1}{|m|!} \frac{\gamma^2}{1 + \gamma^2} e^{-\frac{2F_0}{3F}g(\gamma)} \sum_{q \ge q_{thr}}^{\infty} A_q(\omega, \gamma), \tag{4.64}$$

where  $(2F_0/F)^{2n^*}$  is the correction of the long-range Coulomb interaction given that the Coulomb field is expressed as  $F_0 = (2I_p)^{3/2}$  and the Keldysh number is  $\gamma = \omega \left(F_0^{1/3}/F\right)$ .

The effective principal quantum number  $n^* \equiv Z/\sqrt{2I_p}$ , and the effective orbital quantum number is  $l^* = n^* - 1$ . The three coefficients are

$$|C_{n^*l^*}|^2 = \frac{2^{2n^*}}{n^*\Gamma(n^* + l^* + 1)\Gamma(n^* - l^*)},\tag{4.65}$$

$$G_{lm} = \frac{(2l+1)(l+|m|)!}{2^{|m|}|m|!(l-|m|)!},$$
(4.66)

$$g(\gamma) = \frac{3}{2\gamma} \left[ \left( 1 + \frac{1}{2\gamma^2} \right) \sinh^{-1}(\gamma) - \frac{\sqrt{1 + \gamma^2}}{2\gamma} \right]. \tag{4.67}$$

The value of  $\sum_{q\geq q_{ihr}}^{\infty}A_q(\omega,\gamma)$  can be obtained approximately by setting the upper limit of the sum to  $q_{max}-v=10/\alpha(\gamma)$ . For even larger values

of q, the contribution to the sum can be neglected because  $e^{-\alpha(q-\nu)}$  is much smaller than that of the leading terms.

The unit of the rate  $w_{PPT}$  is the number of electrons per atomic unit of time, which corresponds to  $41.341w_{PPT}/\text{fs}$ . F is also in atomic unit, which can be calculated from the intensity in W/cm<sup>2</sup> by

$$F[\text{a.u.}] = \sqrt{\frac{I[\text{w/cm}^2]}{3.55 \times 10^{16}}}.$$
 (4.68)

Noble gases are commonly used for attosecond pulse generation. Except for helium, the outmost orbital of all four other atoms is the p configuration, whereas it is s for He, as shown in Table 4.1. The outmost electrons are ionized first because of their smaller ionization potential. For example, for the neon atom, the ionization potentials of the 2p and the 2s electron are 21.57 and 48.48 eV, respectively. For the p orbital, the state with m = 0 has larger rate than  $m = \pm 1$  (see Problem 4.10).

The parameters  $|C_{n^*l^*}|^2$  and  $G_{lm}$  of the rare gases are listed in Table 4.2. Here, the state that has the highest ionization rate is shown.

The calculated ionization rate of helium by a laser centered at 790 nm is shown in Figure 4.12. In the intensity range of  $3 \times 10^{13} - 3.5 \times 10^{14}$  W/cm<sup>2</sup>, it agrees well with the results from the numerical solution of the Schrödinger Equation, in the limit  $I \to 0$ ,  $w = \sigma I^q$ , where  $\sigma$  is the cross section, q is the minimum number of photons required to free an electron from an atom. In this case, at low intensities,  $q = 7 \sim 8$ . The contributions of different orders to the rate are plotted in Figure 4.13, at three different intensities.

TABLE 4.1 The Electron Configuration of Noble Gases

	<b>Electron Configuration</b>	<i>I<sub>P</sub></i> (eV)	1	m
Не	$1 s^2$	24.587	0	0
Ne	$1 s^2 2s^2 p^6$	21.564	1	0
Ar	$1 s^2 2s^2 p^6 3s^2 p^6$	15.759 ( $J = 3/2$ )	1	0
		15.936 ( $J = 1/2$ )		
Kr	$1 s^2 2s^2 p^6 3s^2 p^6 d^{10} 4s^2 4p^6$	13.999 ( $J = 3/2$ )	1	0
		14.665 (J = 1/2)		
Хе	$1 s^2 2 s^2 p^6 3 s^2 p^6 d^{10} 4 s^2 p^6 d^{10} 5 s^2 p^6$	12.129 ( $J = 3/2$ )	1	0
		13.436 ( $J = 1/2$ )		

**TABLE 4.2** The ADK Parameters

	F <sub>0</sub> (a.u.)	n*	<i>l</i> *	1	m	$\left  C_{n^*l^*} \right ^2$	G <sub>lm</sub>
He	2.42946	0.74387	-0.25613	0	0	4.25575	1
Ne	1.99547	0.7943	-0.2057	1	0	4.24355	3
Ar	1.24665	0.92915	-0.07085	1	0	4.11564	3
Kr	1.04375	0.98583	-0.01417	1	0	4.02548	3
Xe	0.84187	1.05906	0.05906	1	0	3.88241	3

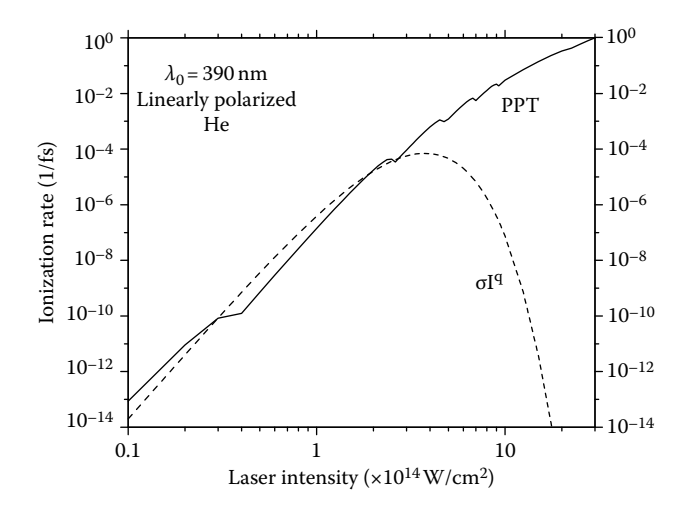


Figure 4.12 PPT rate of helium.

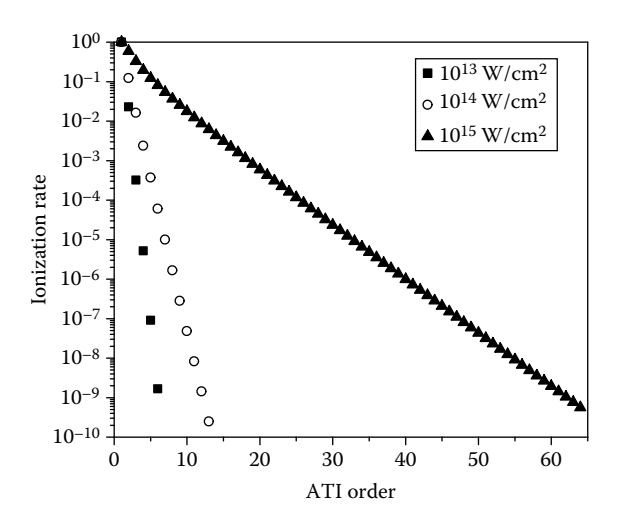


Figure 4.13 Contribution of the first three terms.

#### 4.2.3 ADK Model

Ammosov, Delone, and Krainov derived the expressions for the tunnel ionization probabilities of arbitrary complex atoms and atomic ions. Their theory is essentially an extension of the PPT theory. They took into account that the states of the complex atoms are characterized by the effective principal and orbital quantum numbers. The effective principle quantum number is  $n^* \equiv Z/\sqrt{2I_p}$ , and the effective orbital quantum number is  $l^* = n^* - 1$ .

In the tunneling regime,  $\gamma \ll 1$ , we have  $\left(1/\sqrt{1+\gamma^2}\right)^{-|m|-1} \approx 1$ ,  $\sum_{q \geq q_{thr}}^{\infty} A_q(\omega, \gamma) \approx 1$ , and  $g(\gamma) \approx 1$ . The ionization can be calculated by the ADK rate by the expression

$$w_{ADK} = |C_{n^*l^*}|^2 G_{lm} I_p \left(\frac{2F_0}{F}\right)^{2n^* - |m| - 1} e^{-\frac{2F_0}{3F}}.$$
 (4.69)

When  $\gamma \gg 1$ , the main difference between the PPT and the ADK rate is caused by the  $g(\gamma)$  because it is in the exponent of the PPT rate. As concluded by Ilkov et al., use of the ADK theory should be limited to regions of intensity where  $\gamma$  is smaller than 0.5.

#### 4.2.3.1 Cycle-Averaged Rate

For a linearly polarized laser field with amplitude  $F_a$  and  $2F_0/3F_a \gg 1$ , the cycle-averaged rate is

$$\bar{w}_{ADK}(F_a) = \frac{1}{T_0} \int_0^{T_o} w_{ADK}(t)dt$$

$$\approx |C_{n^*l^*}|^2 G_{lm} I_p \left(\frac{2F_0}{F_a}\right)^{2n^* - |m| - 1} \frac{2}{\pi} \int_0^{\pi/2} e^{-\frac{2F_0}{3F_a|\cos(x)|}} dx. \quad (4.70)$$

The integral

$$\int_{0}^{\pi/2} e^{-\frac{2F_{0}}{3F_{a}|\cos(x)|}} dx \approx \int_{0}^{\infty} e^{-\frac{2F_{0}}{3F_{a}}\cosh(x)} dx = K_{0} \left(\frac{2F_{0}}{3F_{a}}\right)$$

$$\approx \sqrt{\frac{\pi}{2}} \frac{1}{\sqrt{\frac{2F_{0}}{3F_{a}}}} e^{-\frac{2F_{0}}{3F_{a}}}.$$
(4.71)

 $K_0$  in Equation 4.65 is the zero order modified Bessel function of the second kind. The averaged rate therefore becomes

$$\bar{w}_{ADK}(F_a) = \sqrt{\frac{2}{\pi}} \sqrt{\frac{3F_a}{2F_0}} w_{ADK}(F_a).$$
 (4.72)

Since  $\sqrt{2/\pi}\sqrt{3F_a/2F_0}\ll 1$ , the cycle averaged rate is much smaller than a field with constant strength. Thus, in one laser cycle, the ionization probability of a linearly polarized laser is much lower than the circularly polarized field.

## 4.2.3.2 Cycle-Averaged Rate of an Elliptically Polarized Field

An elliptically polarized field can be written as

$$\vec{F}(t) = F_a [\hat{\iota}\cos(\omega t) + \hat{J}\xi\sin(\omega t)]. \tag{4.73}$$

When the ellipticity  $\xi < 1$  and  $1 - \xi \gg F_a/F_0$ , it was shown by PPT that

$$\bar{w}_{ADK}(F_a) = \sqrt{\frac{1}{1-\xi^2}} \sqrt{\frac{2}{\pi}} \sqrt{\frac{3F_a}{2F_0}} w_{ADK}(F_a).$$
 (4.74)

For a linearly polarized field  $\xi = 1$ , Equation 4.74 becomes Equation 4.72.

#### 4.2.3.3 Saturation Ionization Intensity

The ionization probability of a given atom is determined by the quantum state of the electron, and the laser parameters, which can be calculated from the ionization rate by the integral

$$p = 1 - e^{-\int_{-\infty}^{+\infty} w(t)dt}. (4.75)$$

Figure 4.14 shows the probability as a function of peak intensity of several gases. Attosecond pulse generation has been done at the intensity range of  $10^{14} \text{ W/cm}^2$ .

To compare with measured ion yield, the theoretical ion curve is calculated by taking into account the spatial and temporal dependence of the intensity, and consequently the ionization rates in the focal spot region, which is called volume effect.

#### 4.2.4 Attosecond Electron and Photon Pulses

#### 4.2.4.1 Returning Electron Pulse

The shape of the electron pulses that returns the parent ion is related to the ionization rate at the time t' and its corresponding returning time. The relative ADK rate then becomes

$$w(t') = \frac{w_{ADK}(t')}{|C_{n^*l^*}|^2 G_{lm} I_p} = \left[ \frac{2F_0}{F|\cos(\omega t')|} \right]^{2n^* - |m| - 1} e^{-\frac{2F_0}{3F|\cos(\omega t')}}.$$
 (4.76)

As an example, for  $F_0/F = 100$ ,  $n^* = 1$ , m = 0, the ADK rate is

$$w(t') = \frac{200}{|\cos(\omega t')|} e^{-\frac{200}{3|\cos(\omega t')|}}.$$
 (4.77)

The relative rate in the 0–1 cycle range is shown in Figure 4.15. It can be seen that the ionization rate for the long trajectory  $0 < t' < 0.05T_0$  is much

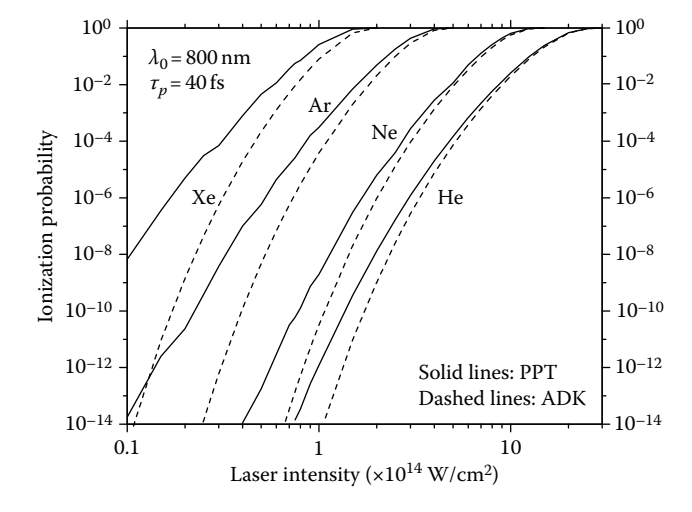


Figure 4.14 Ionization probabilities as a function of peak intensity.

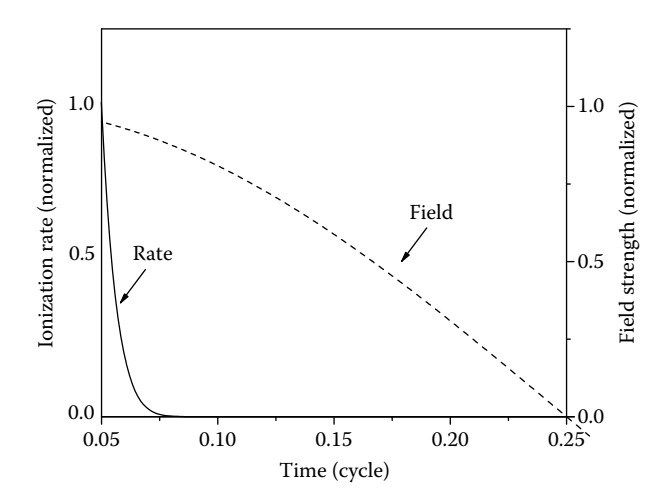


Figure 4.15 The ionization rate for the short trajectory.

larger than that of the short trajectory  $0.05T_0 < t' < 0.25T_0$ . In attosecond experiments, only the short trajectory contributes to the useful photons. The ionization that produces the long trajectory and also the electrons that do not return consume some of the ground-state population, which is not desirable, but unavoidable.

The ionization rate for the short trajectory is shown in Figure 4.15. The ionization rate reduces by 1000 times when t' changes from  $0.05T_0$  to  $0.1T_0$ . Thus, the electrons generated in the range  $0.1T_0 < t' < 0.25T_0$  can be neglected. The returning time range corresponding to  $0.05T_0 < t' < 0.1T_0$  is  $0.57T_0 < t < 0.7T_0$ , which corresponds to 350 as for Ti: Sapphire lasers, which is an indication of the attosecond XUV pulse duration.

#### 4.2.4.2 Attosecond Pulse Train and High-Order Harmonics

Figure 4.16 shows that the ionization rate has two maxima in each laser cycle, which indicates that there a pair of attosecond electron pulses are released per laser cycle. When they return and recombine with the parent ion, two light pulses are emitted. This process repeats from one laser cycle to the next, which results in an attosecond pulse train if the laser pulse contains many optical cycles. The spacing between the two adjacent attosecond pulses is half of a laser cycle. The interference between the pulses in the frequency domain leads to the high-order harmonic peaks.

## 4.3 Cutoff Photon Energy

Cutoff photon energy is one of the most important parameters in high harmonic and attosecond pulse generations. The highest photon energy achievable when the returning electron recombines with the parent ion is determined by the maximum kinetic energy of the electron as it returns to the nucleus

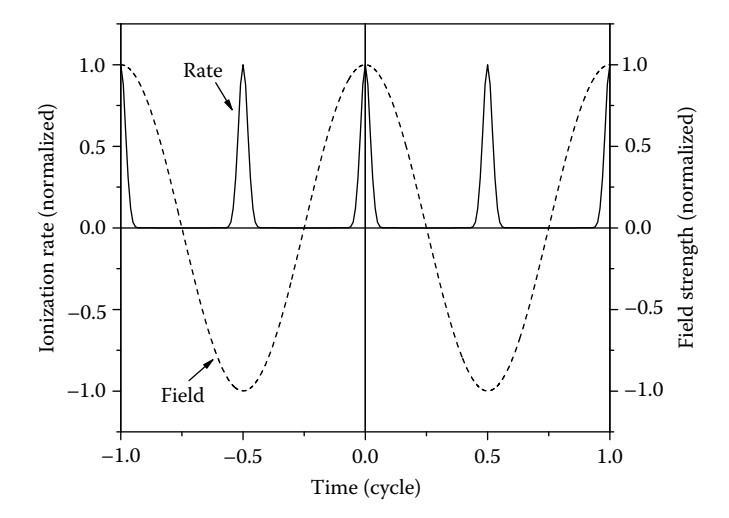


Figure 4.16 The ionization rate in a cosine laser field.

$$\hbar\omega_c = I_p + 3.17U_p,\tag{4.78}$$

where

 $U_p$  is the ponderomotive energy  $I_p$  is the ionization potential of the atom

Since the ponderomotive energy is proportional to the laser intensity, this equation seems to indicate that the cutoff photon energy can be increased to any desired value with enough high laser intensity. Unfortunately, this is not true. It is also wrong to think that the cutoff photon energy depends linearly on the ionization potential as the equation indicates.

The light emission from recombination is a quantum process. The coherent XUV radiation is generated by the superposition of the returning electron wave and the ground state electron wave. The ground-state population should not be depleted completely when the freed electron wave returns, which is discussed in detail in Chapter 5. For a pulse laser field, ground-state population can be completely depleted by a portion of the leading edge as depicted in Figure 4.17, leaving no population for the peak portion of the laser pulse. This means that for a given type of atom, there is a maximum laser intensity that ground state can experience. Such intensity is called the saturation intensity, as introduced in Section 4.2.4.

When the depletion of the ground-state population by ionization is taken into account, the above equation becomes

$$\hbar\omega_c = I_p + 3.17 U_p(I_S),$$
 (4.79)

where  $I_S$  is the saturation intensity for the given atom and laser parameters.

## 4.3.1 Saturation Field and Intensity

In the tunneling regime, a simple equation is derived to predict  $\hbar\omega_c$  for given experimental conditions, which shows the explicit dependence of

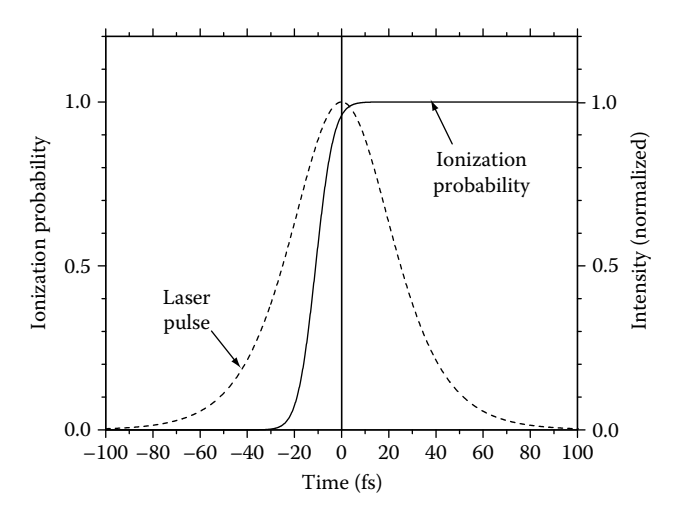


**Figure 4.17** Depletion of the ground-state population by the leading edge of the laser pulse.

the cutoff photon energy on the atomic and laser parameters. Assuming that the atom is ionized by the leading edge of a linearly polarized laser pulse, we first derive the analytical expression of the saturation intensity,  $I_S$ .

#### 4.3.1.1 Sech Square Pulse

For mathematical simplicity, we assume that the shape of the laser field is a hyperbolic secant function peaked at t = 0. The field envelope is expressed as

$$F(t) \propto \operatorname{sech}\left(1.76 \frac{t}{\tau_p}\right),$$
 (4.80)

where  $\tau_p$  is the FWHM of the intensity envelope. Here, we use F instead of E(t) to be consistent with the literatures. Such a pulse is called a sech square pulse in the laser community because for many applications the primary concern is about the intensity profile, which is the square of the electric field. The field envelope of a sech pulse and a Gaussian pulse is shown in Figure 4.18 for comparison. The fields near the peak are very close to each other. Since the ionization occurs mostly near the peak of the pulse, the results we obtain with the sech pulse can also be applied to Gaussian pulses.

#### 4.3.1.2 Definition of Ionization Saturation

To find out the saturation intensity for the case where the atom is almost fully ionized by the leading edge of the pulse, we calculate the ionization probability by the first half of the laser pulse. The ionization probability is

$$p(t) = 1 - p_0(t), (4.81)$$

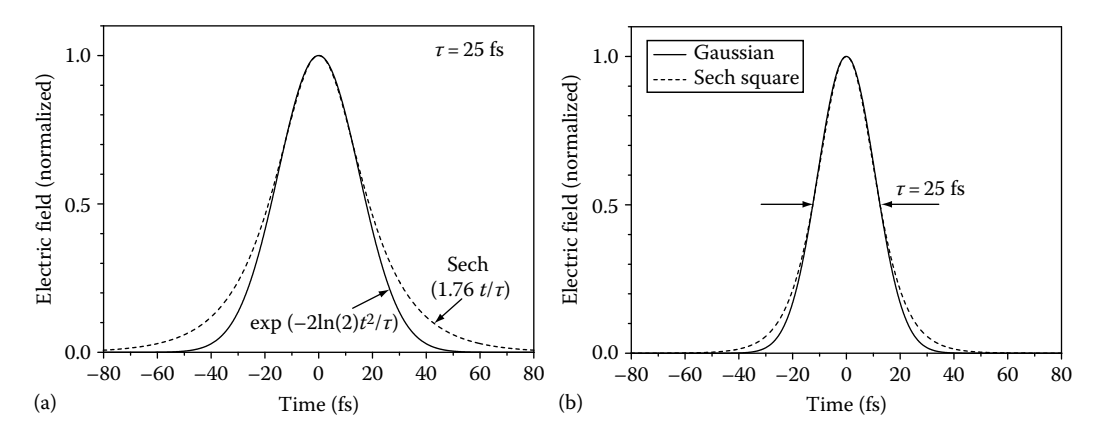


Figure 4.18 Comparison between a sech square pulse and a Gaussian pulse. (a) Field. (b) Intensity.

where  $p_0$  is the ground-state population. The ground-state population and the ionization rate are related by the rate equation by

$$\frac{dp_0}{dt} = -w(t)p_0,\tag{4.82}$$

where w(t) is the ionization rate determined by the instantaneous laser field strength. Consequently, the population at the time of the intensity peak is

$$p_0(t=0) = e^{-\int_{-\infty}^0 w(t)dt}.$$
 (4.83)

Here, we define the saturation intensity,  $I_S$ , at which the ionization probability is  $p_s = p(t=0) = 1 - p_0$  (t=0) = 0.98. In other words, there are only 2% ground-state populations left for generating attosecond pulses after the peak of the pulse, which can be neglected.

#### 4.3.1.3 ADK Rate

In the tunneling regime, the ADK rate can be used. It can be expressed in the form

$$w_{ADK} = \rho \left(\frac{1}{F_1}\right)^{g+1} e^{-\frac{1}{F_1}},\tag{4.84}$$

where 
$$\rho = |C_{n^*l^*}|^2 G_{lm} \frac{2l_p}{2} 3^{2n^* - |m| - 1}, g = 2n^* - |m| - 2, F_1 = \frac{3F}{2F_0}.$$

To perform the integral in Equation 4.83, we case Equation 4.84 into the form

$$w_{ADK} = \rho \left( -\frac{\partial}{\partial \beta} \right)^g \frac{1}{F_1} e^{-\frac{\beta}{F_1}}, \tag{4.85}$$

where  $\beta$  is dummy variable that is set to one at the end of calculation.

#### 4.3.1.4 Circularly Polarized Pulses

Although high harmonics cannot be generated with circularly polarized lasers, it is easy to perform the integral in Equation 4.83 because the field

strength is the same as the field envelope. In other words, there are no fast oscillation terms in the integral. It turns out that the expressions for the saturation intensity of the linearly polarized field is similar to that of the circularly polarized laser.

The quantity,  $F_1$ , related to the field strength can be expressed as

$$F_1(t) = \frac{3F(t)}{2F_0} = F_{10} \operatorname{sech}\left(1.76 \frac{t}{\tau_p}\right).$$
 (4.86)

The integral is therefore

$$\int_{-\infty}^{0} w(t)dt$$

$$= \rho \int_{-\infty}^{0} \left( -\frac{\partial}{\partial \beta} \right)^{g} \frac{1}{F_{10} \operatorname{sech} \left( 1.76 \frac{t}{\tau_{p}} \right)} e^{-\frac{\beta}{F_{10} \operatorname{sech} \left( 1.76 \frac{t}{\tau_{p}} \right)}} dt$$

$$= \rho \frac{\tau}{1.76} \left( -\frac{\partial}{\partial \beta} \right)^{g} \frac{1}{F_{10}} \int_{-\infty}^{0} \frac{1}{\operatorname{sech} \left( 1.76 \frac{t}{\tau_{p}} \right)} e^{-\frac{\beta}{F_{10} \operatorname{sech} \left( 1.76 \frac{t}{\tau_{p}} \right)}} d\left( 1.76 \frac{t}{\tau_{p}} \right)$$

$$= \rho \frac{\tau}{1.76} \left( -\frac{\partial}{\partial \beta} \right)^{g} \left[ \frac{1}{F_{10}} K_{1} \left( \frac{\beta}{F_{10}} \right) \right]. \tag{4.87}$$

 $K_1$  in Equation 4.87 is the first order modified Bessel function of the second kind. For the field used in tunneling ionization  $1/F_{10} = \beta/F_{10} \gg 1$ , we have

$$K_1\left(\frac{\beta}{F_{10}}\right) \approx \sqrt{\frac{\pi}{2}} \frac{1}{\sqrt{\frac{\beta}{F_{10}}}} e^{-\frac{\beta}{F_{10}}}.$$
 (4.88)

 $K_1$  (x) and its asymptotic expression are plotted in Figure 4.19.

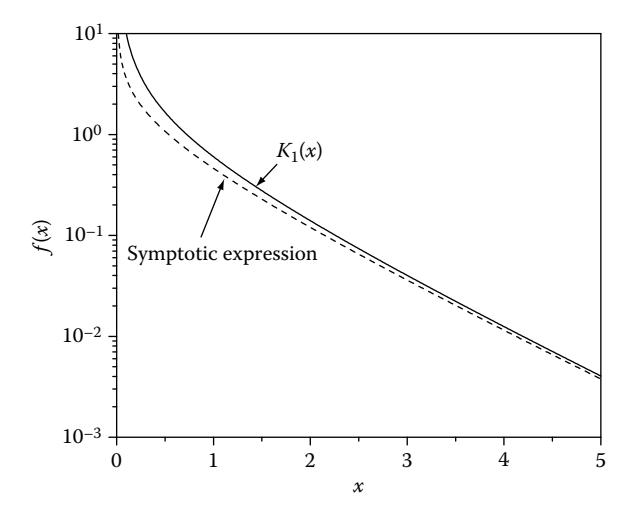


**Figure 4.19** Graph of  $K_1(x)$  and its asymptotic expression.

Since

$$-\frac{d}{dx}\left(\frac{1}{\sqrt{x}}e^{-x}\right) = \left(\frac{1}{2x} + 1\right)\frac{1}{\sqrt{x}}e^{-x} \approx \frac{1}{\sqrt{x}}e^{-x}, \quad x \gg 1, \tag{4.89}$$

We have

$$\left(-\frac{\partial}{\partial \beta}\right)^{g} \left(\frac{1}{\sqrt{\frac{\beta}{F_{10}}}} e^{-\frac{\beta}{F_{10}}}\right) = \frac{1}{F_{10}} \frac{1}{\sqrt{\frac{\beta}{F_{10}}}} e^{-\frac{\beta}{F_{10}}}.$$
 (4.90)

Set  $\beta = 1$ , the integral

$$\int_{-\infty}^{0} w(t)dt \approx |C_{n^*l^*}|^2 G_{lm} I_p 3^{2n^* - |m| - 1} \frac{\tau_p}{1.76} \sqrt{\frac{\pi}{2}} \frac{1}{F_{10}^{3/2}} e^{-\frac{1}{F_{10}}}.$$
 (4.91)

Thus,

$$-\ln(1-p_s) = |C_{n^*l^*}|^2 G_{lm} I_p 3^{2n^*-|m|-1} \frac{\tau_p}{1.76} \sqrt{\frac{\pi}{2}} \frac{1}{F_{10}^{3/2}} e^{-\frac{1}{F_{10}}}, \tag{4.92}$$

which can be expressed as

$$F_{10} = \frac{1}{\ln \left[ \frac{|C_{n^*l^*}|^2 G_{lm} I_p 3^{2n^* - |m| - 1} \frac{\tau_p}{1.76} \sqrt{\frac{\pi}{2} \frac{1}{F_{10}^{3/2}}}}{-\ln(1 - p_s)} \right]}.$$
 (4.93)

By definition

$$F_{10} = \frac{3F_S}{2F_0} = \frac{3F_s}{2(2I_0)^{\frac{3}{2}}},\tag{4.94}$$

where  $F_s$  is field strength corresponding to the saturation intensity,  $I_s$ .

In the denominator, we make an approximation:  $F_{10} = 1$ . The saturation field peak amplitude can then be expressed as

$$F_{s} = \frac{\frac{2}{3} (2I_{p})^{\frac{3}{2}}}{\ln \frac{|C_{n^{*}l^{*}}|^{2} G_{lm} I_{p} 3^{2n^{*} - |m| - 1}}{-\ln (1 - p_{s})}}.$$
(4.95)

It is important to keep in mind the quantities in this equation are in atomic units.

#### 4.3.1.5 Linearly Polarized Fields

Attosecond pulse cannot be generated by circularly polarized laser because the returned electron misses the parent ion in such a laser field, which is discussed later in this chapter. For linearly polarized laser, we use the cycle-averaged ionization rate to calculate the saturation intensity, which is

$$\bar{w}_{ADK}(F_{10}) = \sqrt{\frac{2}{\pi}} \sqrt{F_{10}} w_{ADK}(F_{10}).$$
 (4.96)

Following the same procedure as the case of circular polarization, we can get the saturation field when the atom is ionized by a linearly polarized laser

$$F_{s} = \frac{\frac{2}{3}(2I_{p})^{\frac{3}{2}}}{\ln \frac{\left|C_{n^{*}l^{*}}\right|^{2}G_{lm}I_{p}3^{2n^{*}-|m|-1}\frac{\tau_{p}}{1.76}\frac{1}{F_{10}}}{-\ln(1-p_{s})}}.$$
(4.97)

Again, making the approximation  $F_{10} = 1$  in the denominator, we have

$$F_{s} = \frac{\frac{2}{3} (2I_{p})^{\frac{3}{2}}}{\ln \frac{\left|C_{n^{*}l^{*}}\right|^{2} G_{lm} I_{p} 3^{2n^{*} - |m| - 1}}{-\ln (1 - p_{s})}}.$$
(4.98)

#### 4.3.1.6 Saturation Intensity for Linearly Polarized Field

The atomic unit of intensity is defined as that at which the laser field amplitude is one atomic unit. Thus, the saturation intensity in atomic unit is

$$I_{s} = F_{s}^{2} = \frac{\frac{32}{9}I_{p}^{3}}{\left[\ln\frac{|C_{n^{*}l^{*}}|^{2}G_{lm}I_{p}3^{2n^{*}-|m|-1}\frac{\tau_{p}}{1.76}}{-\ln(1-p_{s})}\right]^{2}}.$$
 (4.99)

For experimentalists, it is more convenient to use  $W/cm^2$  for intensity. One atomic unit of intensity corresponds to  $3.55 \times 10^{16}$   $W/cm^2$ . One commonly uses eV for ionization potential, and fs for pulse duration. In such units, the saturation intensity becomes

$$I_{s} = \frac{6.27I_{p}^{3}}{\left[\ln\frac{0.86|C_{n^{*}l^{*}}|^{2}G_{lm}I_{p}3^{2n^{*}-|m|-1}\tau_{p}}{-\ln(1-p_{s})}\right]^{2}} \times 10^{12} \,\mathrm{W/cm^{2}}.$$
 (4.100)

This equation is derived by making the approximation  $F_{10} = 1$  in the denominator of the saturation field. It can be modified slightly to have better agreement to the saturation intensity calculated by integrating the ADK rate numerically. The modified expression is

$$I_{s} = \frac{1.7I_{p}^{3.5}}{\left[\ln\frac{0.86|C_{n^{*}l^{*}}|^{2}G_{lm}I_{p}3^{2n^{*}-|m|-1}\tau_{p}}{-\ln(1-p_{s})}\right]^{2}} \times 10^{12} \,\mathrm{W/cm^{2}}.$$
 (4.101)

#### 4.3.1.7 Ionization Probability

 $p_s$  is the ionization probability at the peak of pulse (t=0), which is important for attosecond and high harmonic generation. For some other applications, we need to know the ionization probability at the end of pulse  $(t=\infty)$ , which is

$$p = 1 - e^{-\int_{-\infty}^{\infty} w(t)dt}. (4.102)$$

For a linearly polarized laser, the rate integral in atomic units is

$$\int_{-\infty}^{\infty} w(t) = \frac{2}{1.76} \tau_p |C_{n^*l^*}|^2 G_{lm} I_p 3^{2n^* - |m| - 1} \frac{1}{F_{10}} e^{-\frac{1}{F_{10}}}$$

$$= 1.14 \tau_p \frac{(3F_{10})^{2n^* - |m| - 1}}{F_{10}} W_{ADK}(F_{10}). \tag{4.103}$$

Thus

$$p_L(F_{10}) = 1 - e^{-1.14\tau_p \frac{(3F_{10})^{2n^* - |m| - 1}}{F_{10}} W_{ADK}(F_{10})},$$
(4.104)

where

$$F_{10} = \frac{3F_a}{2F_0} = \frac{3F_a}{2(2I_p)^{\frac{3}{2}}}. (4.105)$$

Equation 4.104 can be revised to Equation 4.106 by fitting the results from the numerical integration of the ionization rate,

$$p_L(F_{10}) = 1 - e^{-1.14\tau_p 3^{2n^* - |m| - 1} F_{10}^{2.41} W_{ADK}(F_{10})}.$$
 (4.106)

The comparison of the ionization probability calculated by the PPT, ADK, and Equation 4.106 is shown in Figure 4.20. It can be seen that the

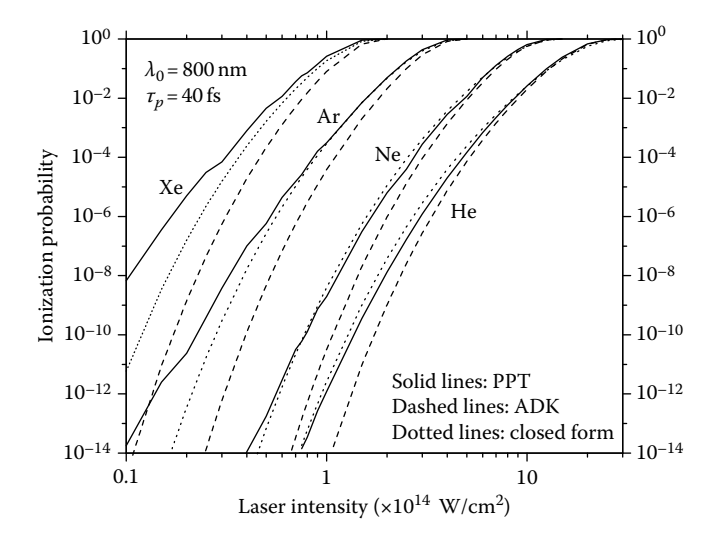


Figure 4.20 Ionization probability calculated with three expressions.

probability calculated by Equation 4.106 is closer to the PPT results, which is more precise than the ADK results. This equation allows us to estimate the ionization probability without performing the integral numerically.

It is also interesting to compare Equation 4.106 with that corresponding to a square pulse with duration  $\tau$ , which is

$$p_L(F_{10}) = 1 - e^{-\tau_p \bar{w}_{ADK}(F_{10})}. (4.107)$$

For circularly polarized laser pulse, the rate integral in atomic units is

$$\int_{-\infty}^{\infty} w(t) = \frac{2}{1.76} \tau_p |C_{n^*l^*}|^2 G_{lm} I_p 3^{2n^* - |m| - 1} \sqrt{\frac{\pi}{2}} \frac{1}{F_{10}^{3/2}} e^{-\frac{1}{F_{10}}}$$

$$= 1.42 \tau_p \frac{(3F_{10})^{2n^* - |m| - 1}}{F_{10}^{3/2}} W_{ADK}(F_{10}). \tag{4.108}$$

By fitting the results with numerical integration of the ionization rate, we obtain the revised expression

$$p(F_{10}) = 1 - e^{-1.42\tau_p 3^{2n^* - |m| - 1} F_{10}^{1.91} W_{ADK}(F_{10})}.$$
 (4.109)

## 4.3.2 Cutoff due to Depletion of the Ground State

To calculate the cutoff photon energy of the high harmonic or attosecond pulse spectrum set by the depletion of the ground state, we substitute

$$I_{s} = \frac{1.7I_{p}^{3.5}}{\left[\ln\frac{0.86|C_{n^{s}I^{*}}|^{2}G_{lm}I_{p}3^{2n^{*}-|m|-1}\tau_{p}}{-\ln(1-p_{s})}\right]^{2}} \times 10^{12} \text{ W/cm}^{2}.$$
 (4.110)

into

$$\hbar\omega_c = I_p + 3.17 \ U_p(I_S),$$
 (4.111)

where  $U_p(I_s) = 9.33 \times 10^{14} I_s \lambda^2$ . Finally, we obtain an expression for the cutoff photon energy

$$\hbar\omega_c = I_p + \frac{0.5I_p^{3.5}\lambda^2}{\left[\ln\left(\frac{0.86I_p3^{2n^*-1}G_{lm}C_{n^*l^*}^2}{-\ln(1-p_S)}\tau_p\right)\right]^2},$$
(4.112)

where  $p_S$  is the ionization probability at the peak of the pulse that defines the saturation of the ionization of the ground-state population, which can be set to 0.98. The unit of  $\hbar\omega_c$  and  $I_p$  is eV,  $\lambda$  is  $\mu$ m, and  $\tau_p$  is fs. The values of  $n^*$ ,  $G_{lm}$ , and  $C^2_{n^*l^*}$  associated with the quantum parameters of the ground state are found in Table 4.2. Equation 4.112 shows the explicit dependence of the cutoff photon energy on the atomic and laser

parameters. Most importantly, it includes the effects of the ground-state depletion by the leading edge of the driving laser pulse.

To increase the cutoff, we can use atoms or ions that have high ionization potential, or lasers with short pulse duration and long wavelength. The  $\hbar\omega_c$  value also determines the shortest attosecond pulses that can be generated.

#### 4.3.2.1 Ionization Potential

Equation 4.112 indicates that the cutoff photon energy should be proportional to approximately the cube of the ionization potential of the atom, i.e.,  $I_p^{3.5}$ . This is because, for a given laser-pulse duration, it is much harder to deplete the ground state of the atoms with a larger ionization potential. As the ADK theory revealed, the ionization rate is an exponential function of the ionization potential.

Experimentally, using 25 fs lasers centered at 800 nm, harmonics up to 29, 41, 61, and 155 have been generated Xe, Kr, Ar, and Ne, with corresponding ionization potentials of 12.13, 13.99, 15.76, and 21.56 eV, respectively, as shown in Figure 4.21. Using Equation 4.112, we can predict that harmonics up to the order of 27, 41, 61, and 163 should be observed from Xe, Kr, Ar, and Ne, respectively. The simple calculations and experimental observations are, therefore, in very good agreement. The measured cutoff order can be lower than the predicted value due to plasma induced defocusing and phase mismatch, which are not included when Equation 4.112 is derived. Phase matching is discussed in Chapter 6. In the experiments, the gas pressure was kept at very low to minimizing the plasma effects.

Ions have even higher ionization potential, and thus it is possible to generate even higher harmonic order from ions. However, preparing pure ion targets (not a plasma) with high density is not as easy as it is for neutral ones.

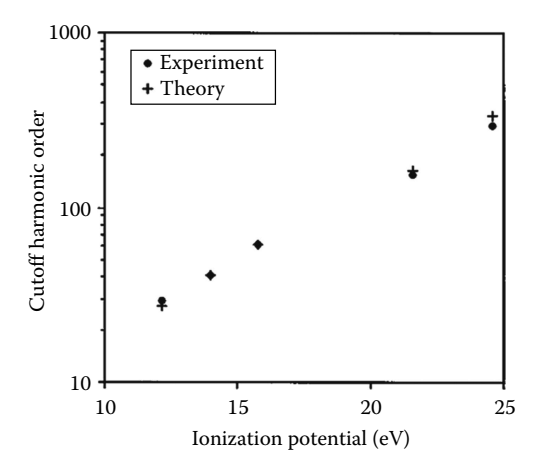


**Figure 4.21** Comparison of predicted and observed cutoff photon energies for harmonic generation in the noble gases (on a log scale). (From Z. Chang, A. Rundquist, H. Wang, H. Kapteyn, and M. Murnane, *Phys. Rev. Lett.*, 79, 2967, 1997. Copyright 1997 by the American Physical Society.)

#### 4.3.2.2 Pulse Width

Equation 4.112 reveals that the cutoff photon energy is inversely proportional to the square of the logarithm of the laser-pulse width, so it is clear that using shorter duration laser pulses should result in the generation of higher order harmonics. At the same laser intensity, a pulse with shorter duration causes less ground-state depletion. Thus atoms can experience higher laser intensity when the pulse is shorter, which leads to higher cutoff photon energy.

This is clearly shown in Figure 4.22, which plots the theoretical predictions for an argon atom, for pulse durations in the range between 10 and 100 fs. For even shorter pulse duration, the carrier-envelope phase also affects the cutoff photon energy, which is not taken into account when deriving Equation 4.112.

For example, when Ti:Sapphire laser system generating 26 fs pulses with a center wavelength of 800 nm is used, we expect to observe harmonics up to order 333 from He, which is well within the "water window" region between 4.4 and 2.3 nm, where water is less absorbing than carbon. X-rays in this region are important for imaging live biology samples. The experimentally generated high harmonic spectrum after a 0.4  $\mu$ m carbon filter is shown in Figure 4.23. The signals below the 155th order are truncated for they are out the measurement range of the spectrometer. The signals above the 183rd order are blocked by the carbon filter. The 155th to 183rd order harmonics are seen as the small intensity modulation on a logarithmic scale. This water window x-ray generation experiment was done in 1997 using a 25 fs Ti:Sapphire CPA laser. Even shorter wavelength XUV light has been generated with 5 fs lasers from hollow-core fiber compressors.

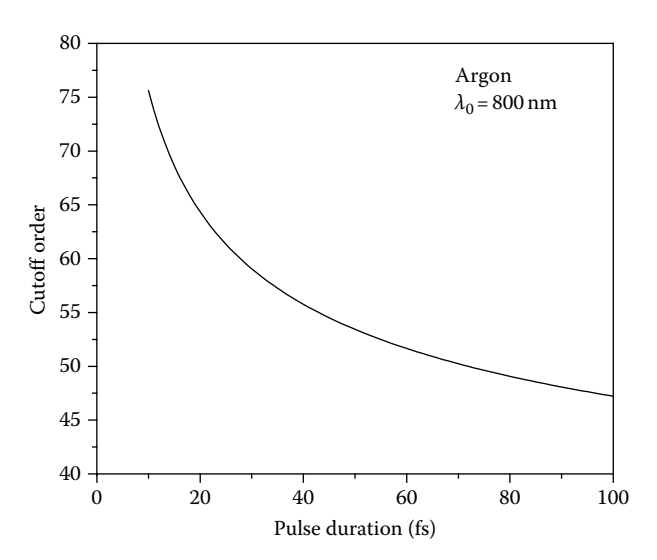
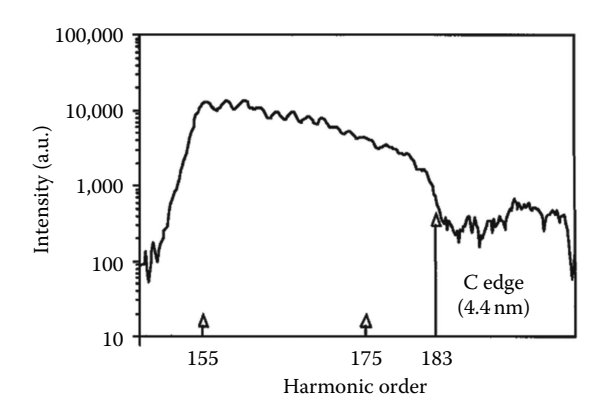


Figure 4.22 Dependence of cutoff order on pulse duration.



**Figure 4.23** Harmonic emission from helium filtered through a  $0.4~\mu m$  carbon filter. (From Z. Chang, A. Rundquist, H. Wang, H. Kapteyn, and M. Murnane, *Phys. Rev. Lett.*, 79, 2967, 1997. Copyright 1997 by the American Physical Society.)

#### 4.3.2.3 Wavelength of the Driving Laser

It is clear in Equation 4.112 that the cutoff photon energy for a given atomic state is proportional to the square of the wavelength. Figure 4.24 shows the calculation results of the relationship between the cutoff photon energy with the driving field wavelength for fixed pulse duration (25 fs). The figure shows that by changing the driving field wavelength from 0.4 to 4  $\mu m$ , the cutoff of helium is extended from 0.2 to more than 10 keV. A Gaussian spectrum with 2 keV FWHM bandwidth supports pulses shorter than 1 as! We can thus expect that Zeptosecond pulses be generated using mid-infrared laser in the future.

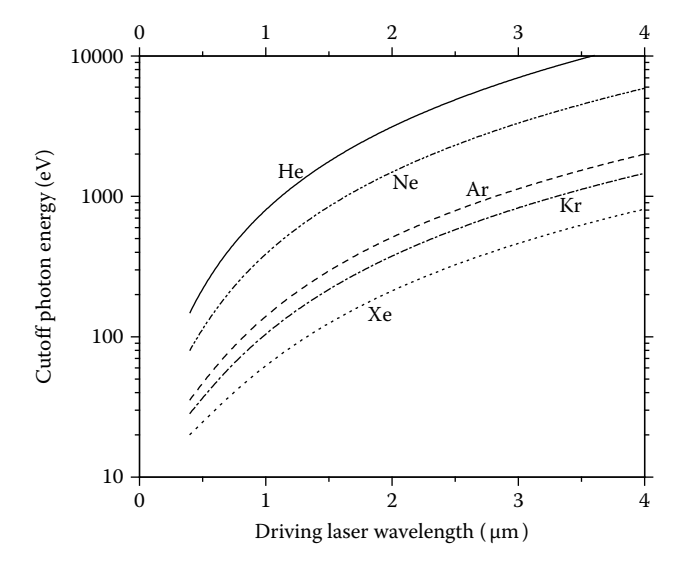


**Figure 4.24** Calculated relationship between single-atom HHG cutoff photon energy and the driving wavelength.

The extension of the cutoff photon energy can be understood with the semiclassical three-step model. In the tunneling ionization regime, the ionization rate is independent of the laser wavelength. Therefore, the saturation intensity is the same for pulses with the same duration but different wavelengths. As a result, electrons experience the same field strength at saturation intensities for pulses with different wavelengths. From Newton's laws of mechanics, we know the kinetic energy of an electron acquired in a given electric field is proportional to the square of the travel time in the field. Therefore, the electrons can gain four times more energy when the optical period of the laser is doubled, or the laser wavelength is two times longer.

The first experiments that demonstrate the extension of the cutoff photon energy of the XUV spectrum by using long-wavelength lasers were demonstrated in 2001. The main difficulty of performing such an experiment is the lack of high-power femtosecond lasers with center wavelength above 1  $\mu m$ . The experiment was performed using an optical parametric amplifier (OPA) instead. It is pumped with a Ti:Sapphire CPA laser that delivered 25 fs, 1.2 mJ at sub-kilohertz repetition rate, as depicted in Figure 4.25. The OPA generates up to 100  $\mu J$  infrared pulses that are tunable from 1.1 to 1.6  $\mu m$ . The OPA pulse duration is also 25 fs.

Because of the low pulse energy, the OPA beam is tightly focused onto the pulsed gas jet to achieve the required intensity. The focal spot size is  $20~\mu m$  full width at half maximum. The gas density is  $1\times 10^{18}~atoms/cm^3$  in a  $200~\mu m$  interaction region. The generated high harmonic signal is measured by a transmission grating based XUV spectrometer. The XUV beam is dispersed by a 2000~line/mm transmission grating on an MCP imaging detector. Another difficulty of the experiment is caused by the low conversion efficiency from the laser energy to the XUV flux. A low noise, 16 bit cooled charge-coupled device (CCD) camera is used to accumulate the spectrum image.

Figure 4.26 shows the results with Xenon gas at four wavelengths. Figure 4.26a is the spectrum produced by the 0.8  $\mu$ m laser. Figures 4.26b through d are the results produced by the OPA pulses tuned at 1.51, 1.37, and 1.22  $\mu$ m, respectively. The results clearly illustrate the cutoff extension by using longer driving-field wavelength. It is worthy to point out the harmonic signal level drops as the wavelength is increased, which can be explained by the quantum theory of the three-step model.

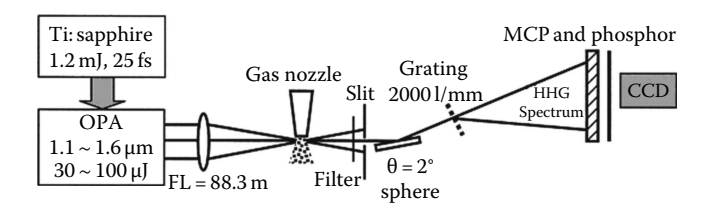


**Figure 4.25** Experimental setup for generating high-order harmonics with long wavelength pump. (From B. Shan and Z. Chang, *Phys. Rev. A*, 65, 011804(R), 2001. Copyright 2001 by the American Physical Society.)

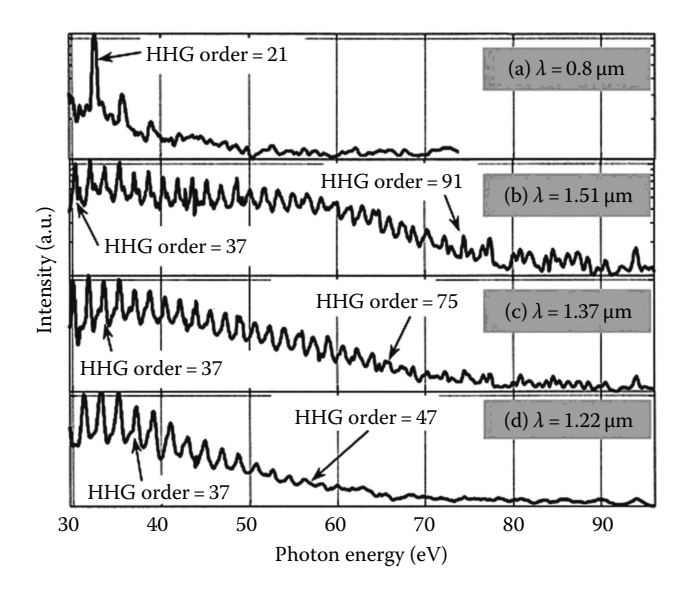


**Figure 4.26** HHG by 50  $\mu$ J, 25 fs laser pulses of different wavelengths in xenon gas. The HHG wavelength is also tuned by the driving wavelength from OPA. (From B. Shan and Z. Chang, *Phys. Rev. A*, 65, 011804(R), 2001. Copyright 2001 by the American Physical Society.)

It is possible to generate 10 keV x-rays by using a 4  $\mu$ m wavelength laser. The optical period corresponds to 4  $\mu$ m is 13.3 fs, thus a 25 fs pulse at this wavelength contains only two cycles! While a 25 fs pulse at 0.8  $\mu$ m can be delivered directly from a Ti:Sapphire CPA laser, generating 25 fs at 4  $\mu$ m is yet to be demonstrated.

#### 4.4 Free Electrons in Two-Color Laser Fields

Attosecond pulses can be generated in the combined laser fields at the fundamental and second harmonic frequencies, which is called two-color field. The generation processes can also be analysed using the three-step model. We first examine the cutoff photon energy of the high harmonic spectrum, which is determined by the kinetic energy of the electron gained in the two-color laser field. The method we use here is very similar to that applied to the one-color field.

## 4.4.1 Equation of Motion

The motion of free electrons in a two-color field can be understood by considering two linearly polarized monochromatic waves with the same polarization direction. The first one is the laser field at the fundamental frequency

$$\varepsilon_1(t) = E_1 \cos(\omega_0 t). \tag{4.113}$$

The second one is the second harmonic (SH) field

$$\varepsilon_2(t) = \alpha E_1 \cos(2\omega_0 t + \phi_{12}), \tag{4.114}$$

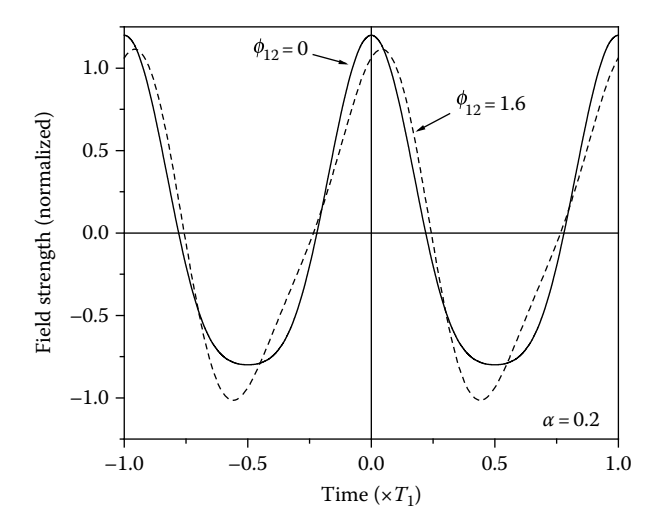


Figure 4.27 The combined two-color field.

where

 $\alpha$  is the ratio of the amplitude of the SH field to that of the  $\omega_0$  field  $\phi_{12}$  is the relative phase between the two fields

The total field is

$$\varepsilon(t) = E_1[\cos(\omega_0 t) + \alpha\cos(2\omega_0 t + \phi_{12})]. \tag{4.115}$$

Figure 4.27 shows the total field for  $\alpha = 0.20$ ,  $\phi_{12} = 0$  and  $\phi_{12} = 1.6\pi$ . The intensity of the SH beam is 4%, i.e.,  $\alpha^2$ , of the fundamental beam.

The equation of motion of a free electron is

$$\frac{d^2x}{dt^2} = -\frac{e}{m}E_1[\cos(\omega_0 t) + \alpha\cos(2\omega_0 t + \phi_{12})]. \tag{4.116}$$

Assuming an electron is freed at time t', and the initial velocity is zero, then the solution of the equation is

$$v(t) = -\frac{eE_{1}}{m\omega_{0}} \left[ \sin(\omega_{0}t) - \sin(\omega_{0}t') + \frac{\alpha}{2} \left[ \sin(2\omega_{0}t + \phi_{12}) \right] \right]$$

$$-\sin(2\omega_{0}t' + \phi_{12}) \right],$$

$$x(t) = \frac{eE_{1}}{m\omega_{0}^{2}} \left\{ \left[ \cos(\omega_{0}t) - \cos(\omega_{0}t') \right] + \frac{\alpha}{4} \left[ \cos(2\omega_{0}t + \phi_{12}) \right]$$

$$-\cos(2\omega_{0}t' + \phi_{12}) \right] + \omega_{0} \left[ \sin(\omega_{0}t') \right]$$

$$+ \frac{\alpha}{2} \sin(2\omega_{0}t' + \phi_{12}) \left[ (t - t') \right],$$

$$(4.118)$$

where v is the velocity of the electron. We define  $x_1 = 2eE_1/m\omega_0^2$ . Equation 4.118 can be normalized to

$$\frac{x(t)}{x_1} = \frac{1}{2} \left\{ \left[ \cos(\omega_0 t) - \cos(\omega_0 t') \right] + \frac{\alpha}{4} \left[ \cos(2\omega_0 t + \phi_{12}) \right] - \cos(2\omega_0 t' + \phi_{12}) \right] + \omega_0 \left[ \sin(\omega_0 t') \right] + \frac{\alpha}{2} \sin(2\omega_0 t' + \phi_{12}) \left[ (t - t') \right].$$
(4.119)

#### 4.4.1.1 Return Time

Return time can be understood by employing a graphic method to examine

$$\left[ \cos(\omega_0 t) + \frac{\alpha}{4} \cos(2\omega_0 t + \phi_{12}) \right] - \left[ \cos(\omega_0 t') + \frac{\alpha}{4} \cos(2\omega_0 t' + \phi_{12}) \right]$$

$$= -\omega_0 \left[ \sin(\omega_0 t') + \frac{\alpha}{2} \sin(2\omega_0 t' + \phi_{12}) \right] (t - t').$$
(4.120)

This is accomplished by plotting the function of the left side as an assistant curve and its tangent at t=t'. The solution is the point where the curve and the line cross, as shown in Figure 4.28. Since  $\alpha/4$  is a small quantity, the function is similar to the fundamental field. Thus, the return time for a two-color system is not very different from the one-color values. However, unlike the one-color case, the function on the left side is not the same function as the two-color laser field. When the relative phase changes, the laser field changes significantly, but the assistant curve does not change much because of the  $\alpha/4$  factor.

By solving the equation x(t) = 0 numerically, we find the return time for  $\phi_{12} = 0$  and  $\phi_{12} = \pi$ , as shown in Figure 4.29. These results are slightly different from the one-color case and it is clear the return time depends on the relative phase  $\phi_{12}$  and the relative amplitude  $\alpha$ .

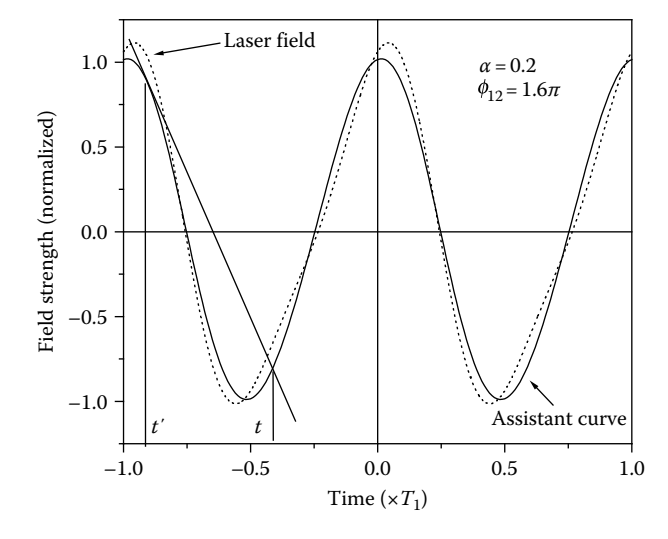


**Figure 4.28** Finding the return time in a two-color laser field graphically,  $\phi_{12} = 1.6\pi$ .

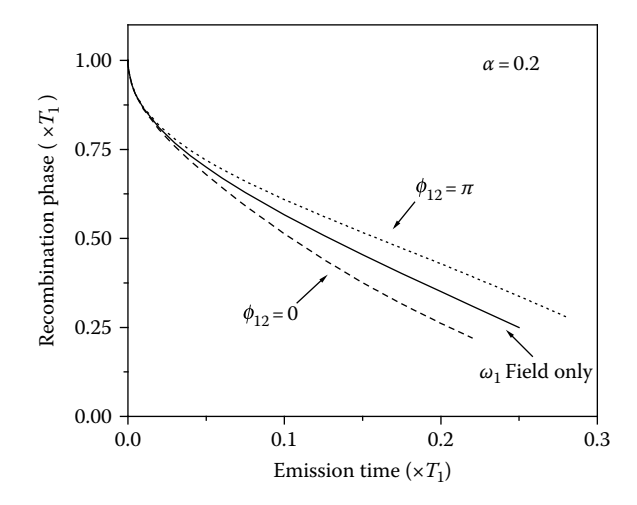


**Figure 4.29** Return time for two relative phases,  $\phi_{12} = 0$  and  $\phi_{12} = \pi$ .

# 4.4.2 Return Energy

The returning velocity can be written as

$$v(t) = v_1(t) + v_2(t),$$
 (4.121)

where  $v_1(t)$  and  $v_2(t)$  are the velocities when only the  $\omega_0$  or the  $2\omega_0$  is present. The velocities can be expressed as

$$v_1(t) = -\frac{eE_1}{m\omega_0} \left[ \sin(\omega_0 t) - \sin(\omega_0 t') \right], \tag{4.122}$$

$$v_2(t) = -\frac{e\alpha E_1}{m2\omega_0} \left[ \sin\left(2\omega_0 t + \phi_{12}\right) - \sin\left(2\omega_0 t' + \phi_{12}\right) \right]. \tag{4.123}$$

Consequently, the returning energy can be expressed as

$$K(t) = \frac{1}{2}m[v_1(t) + v_2(t)]^2 = K_1(t) + K_2(t) + 2\sqrt{K_1(t)K_2(t)}, \quad (4.124)$$

where  $K_1(t)$  and  $K_2(t)$  are the kinetic energy acquired by the electron in the  $\omega_0$  or the  $2\omega_0$  fields, respectively.  $K_2(t)$  depends on the relative phase  $\phi_{12}$ . These two energies normalized to the ponderomotive energy of the  $\omega_0$  field  $U_{p1}$  are

$$\frac{K_1(t)}{U_{p1}} = 2[\sin(\omega_0 t) - \sin(\omega_0 t')]^2,$$
(4.125)

$$\frac{K_2(t)}{\alpha^2 U_{p1}} = \left[\sin\left(2\omega_0 t + \phi_{12}\right) - \sin\left(2\omega_0 t' + \phi_{12}\right)\right]^2. \tag{4.126}$$

Notice that Equation 4.125 has the same form as the one-color case. However, for the same emission time, the return time in the two-color field is different from that in the one-color field (Figure 4.30). As a result, the maximum kinetic energy gain from the fundamental field,  $K_{1,max}$ , is different from the  $3.17U_p$ , as shown in Figure 4.31. For a numerical reference,  $K_{1,max} = 3.47U_p$  for  $\phi_{12} = 1.6\pi$ , whereas  $K_{1,max} = 2.81U_p$  for  $\phi_{12} = 0.6\pi$ .

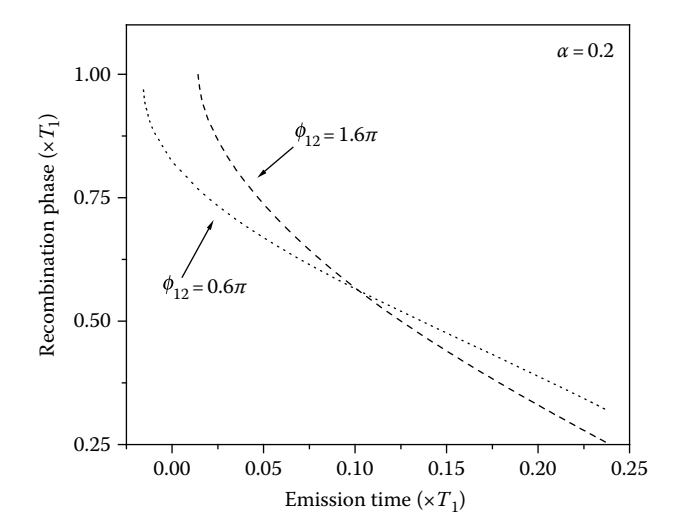


**Figure 4.30** Return time for two relative phases,  $\phi_{12} = 0.6\pi$  and  $\phi_{12} = 1.6\pi$ .

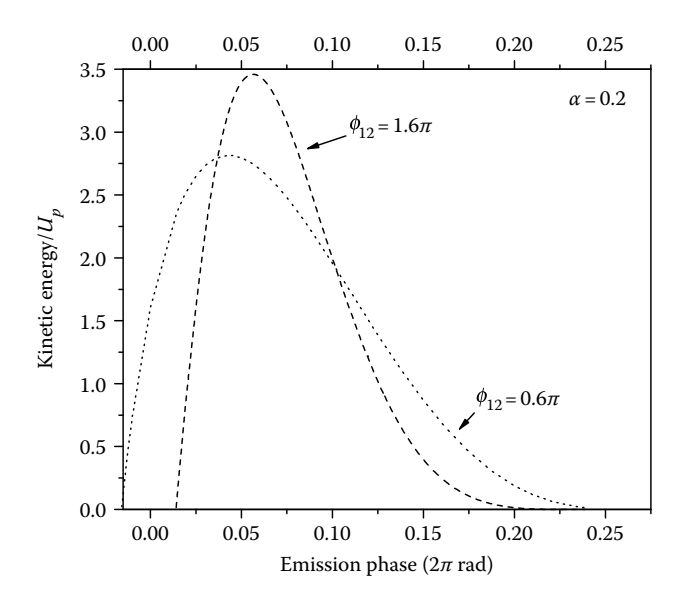


**Figure 4.31** Kinetic-energy component  $K_1(t)$ .

 $K_2(t)/\alpha^2 U_{p1}$  is plotted in Figure 4.32 for  $\phi_{12} = 0.6\pi$  and  $\phi_{12} = 1.6\pi$ . It is interesting to see the  $K_2(t) \approx 0$  in the cutoff region. The cutoff photon energy is the maximum value of K plus the ionization potential of the atom. We can conclude that adding the SH field at these two phases will not extend the cutoff much.

# 4.4.3 Two-Color Gating

The ionization rate depends on  $\alpha$  and  $\phi_{12}$ . For  $\alpha = 0.20$ ,  $\phi_{12} = 0$  and for  $F_0/E_1 = 100$ ,  $n^* = 1$ , m = 0, the rate is shown in Figure 4.33. It is seen that

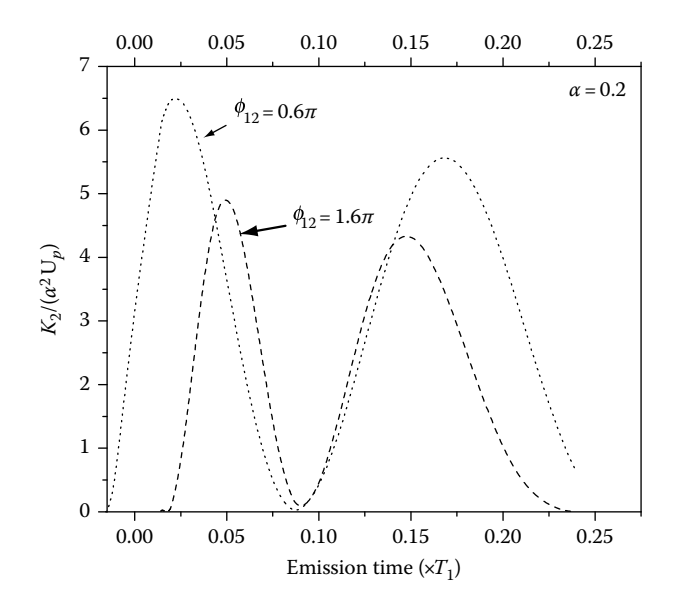


**Figure 4.32** Kinetic-energy component  $K_2(t)$ .

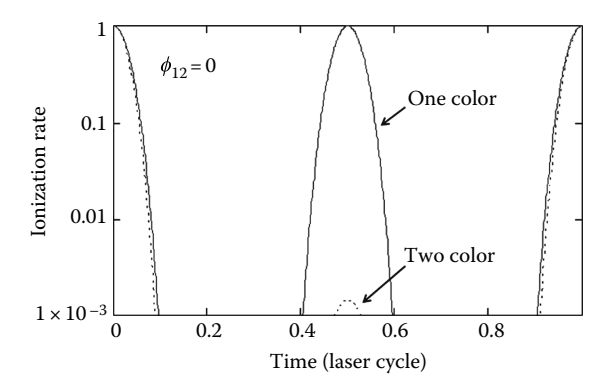


**Figure 4.33** Comparison of the ionization rate between the one-color and the two-color lasers,  $\phi_{12} = 0$ .

the ionization at the half laser cycle is suppressed. Consequently, there will be no attosecond emissions due to the electron emitted there. This increase in the spacing between adjacent attosecond pulses to one laser cycle, which is the foundation of the two-color gating, is discussed in Chapters 7 and 8.

As a comparison, when the relative phase  $\phi_{12} = 1.6\pi$ , the difference between the ionization rate between two maximas of the field is much less than that of the  $\phi_{12} = 0$ , as shown in Figure 4.34.

# 4.5 Polarization Gating

The semiclassical model predicts that when atoms are driven by a linearly polarized femtosecond laser pulse containing multiple optical

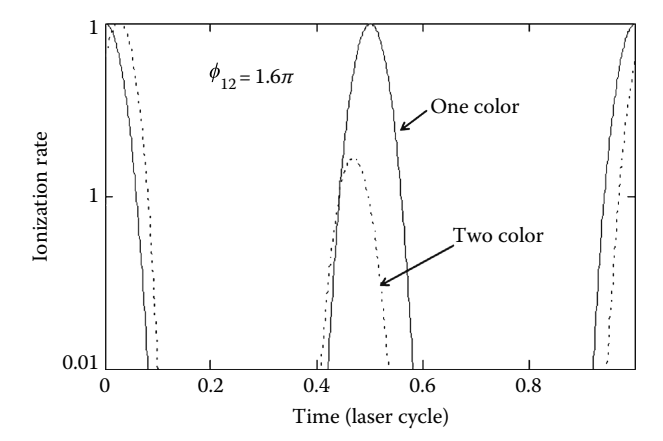


**Figure 4.34** Comparison of the ionization rate between the one-color and the two-color lasers,  $\phi_{12} = 1.6\pi$ .

cycles, a train of attosecond pulses can be generated if the laser intensity is sufficiently high. The three-step process occurs twice a laser cycle, and thus the separation between adjacent pulses is half an optical cycle, which is 1.3 fs for Ti:Sapphire lasers. Attosecond pulse trains are useful light sources for some applications. For cases where the physical processes to be studied last longer than the pulse spacing, it could be hard to interpret the data.

In general, singly isolated attosecond pulses are desirable. When a single attosecond pulse starts the process (the pump) and another attosecond pulse probes it, the time evolution of the system can be mapped out. A scheme for generating single isolated attosecond pulses was first proposed by Corkum in 1994, which is named the polarization gating. It relies on the fact that the attosecond pulse generation efficiency is susceptible to the ellipticity of the driving laser field. It took 12 years for scientists to finally measure the duration of the isolated XUV pulses generated with the polarization gating. In Corkum's the original proposal, two laser pulses with different center frequency are needed. Here, we discuss the principle of polarization gating that requires one center frequency, which is easier to implement experimentally.

# 4.5.1 Electrons in Elliptically Polarized Laser Fields 4.5.1.1 Laser Field

Consider an electric field with ellipticity  $\xi$ , which is defined as the ratio between the amplitude of the minor axis to the major axis of the ellipse that is the trace drawn by the end of the electric vector in a two-dimensional plane as the time increases, as depicted in Figure 4.35. For reference, we define the major axis along the x direction and the minor axis along the y direction. The field can be expressed as

$$\vec{\varepsilon}(t) = E_{x0} \left[ \hat{i} \cos(\omega_0 t) + \hat{j} \xi \sin(\omega_0 t) \right], \tag{4.127}$$

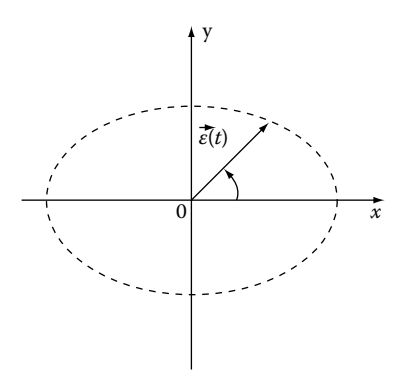


Figure 4.35 Elliptically polarized laser field.

where

 $E_{x0}$  is the amplitude of the major axis  $\hat{i}$  and  $\hat{j}$  are unit vectors in the x and y directions, respectively

The amplitude of the minor axis is  $E_{v0} = \xi E_{x0}$ .

### 4.5.1.2 Equations of Motion

The motion in the x and y directions can be calculated separately as

$$m_e \frac{d^2x}{dt^2} = -eE_{x0}\cos(\omega_0 t) \tag{4.128}$$

and

$$m_e \frac{d^2 y}{dt^2} = -e \xi E_{x0} \sin(\omega_0 t).$$
 (4.129)

The solution of Equation 4.128 is the same as that of the linearly polarized case while the solution of Equation 4.129 is

$$\frac{dy}{dt} = \xi \frac{eE_{x0}}{m\omega_0} \left[ \cos(\omega_0 t) - \cos(\omega_0 t') \right], \tag{4.130}$$

$$y = \xi \frac{eE_{x0}}{m\omega_0^2} [\sin(\omega_0 t) - \sin(\omega_0 t') - \cos(\omega_0 t')\omega_0 (t - t')].$$
 (4.131)

Introducing a normalization factor

$$x_{\text{max}} = \frac{2eE_{x0}}{m\omega_0^2},$$
 (4.132)

which is the maximum displacement in the x direction in one laser cycle, Equation 4.132 becomes

$$\frac{y}{\xi x_{\text{max}}} = \frac{1}{2} \left[ \sin(\omega_0 t) - \sin(\omega_0 t') - \cos(\omega_0 t') \omega_0 (t - t') \right]. \tag{4.133}$$

An example for t' = 0 is shown in Figure 4.36.

The electron released in the range t' = 0 to  $T_0/4$  will return to x = 0, but never returns to y = 0. The trajectory in the x-y plane is shown in Figure 4.37.

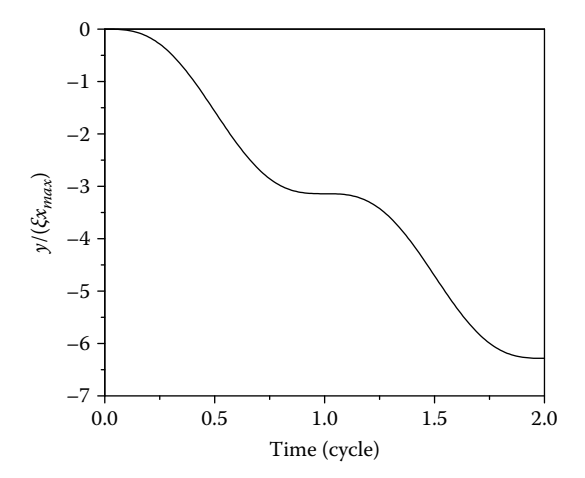
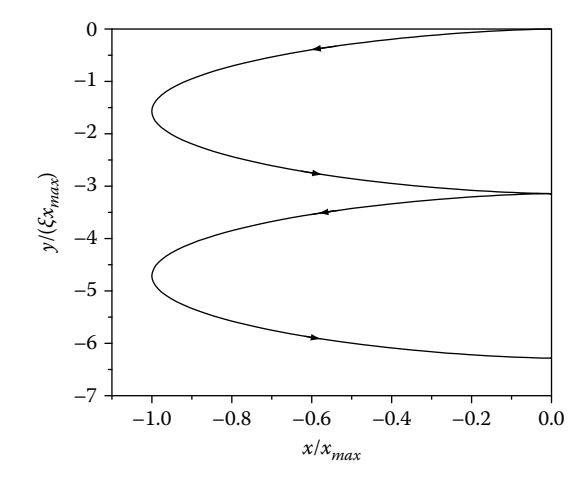


Figure 4.36 The transverse trajectory.



**FIGURE 4.37** The transverse trajectory in the x-y plane.

## 4.5.1.3 Transverse Displacement

For a given electron's birth time, the value of y at the return time in the x direction can be calculated by using Equation 4.133. The numerical solution is shown in Figure 4.38.

The maximum displacement is

$$y_{max} = \pi \xi x_{max}, \tag{4.134}$$

which occurs at t' = 0 or t = T.

The radii of noble gas atoms are listed in Table 4.3. They are on the order of 0.1–0.2 nm. The typical Ti:Sapphire laser intensity for attosecond pulse generation is  $5\times10^{14}$  W/cm<sup>2</sup>,  $x_{max}=2$  nm. For  $\xi=0.1$ ,  $y_{max}\approx0.6$  nm, which is comparable to the atomic radius. For even larger ellipticity, the returning electrons released from an atom will miss the parent ion.

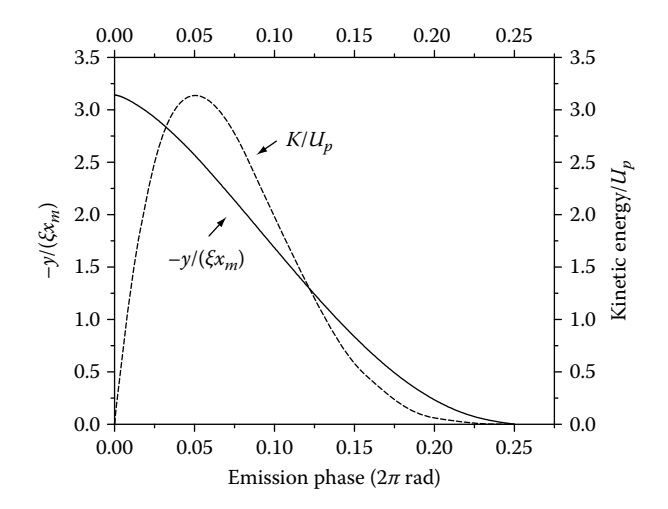


Figure 4.38 The transverse displacement.

TABLE 4.3 Radius of Noble Gas Atoms

	He	Ne	Ar	Kr	Хe
<i>r</i> (nm)	0.130	0.160	0.192	0.198	0.218

#### 4.5.1.4 Quantum Diffusion

Assume the radius of the electron wave packet immediately after tunneling out from an atom is  $r_{\perp}$  and the amplitude of the electron wave function is assumed to be  $e^{-r/r_{\perp}}$ . The transverse velocity can be estimated by the uncertainty principle

$$v_{\perp} = \frac{h}{m_e r_{\perp}}.\tag{4.135}$$

For example, for neon atoms,  $r_{\perp} = \sqrt{2} \times 0.16$  nm and  $v_{\perp} = 3.2$  nm/fs. The width of the wave function increases with time, i.e., equals  $v_{\perp}t + r_{\perp}$ . In a linearly polarized field, the amplitude distribution of the ground state and the returning wave packet after one laser cycle (2.67 fs) is shown in Figure 4.39. In a circularly polarized field ( $\xi = 1$ ), the amplitude is shown in Figure 4.40.

The quantum diffusion leads to the reduction of laser attosecond pulse conversion efficiency. However, it allows the recombination to occur even when ellipticity is larger than 0.1. When the ellipticity increases, the amplitude of the part of the returning electron that meets the parent ion decreases. That is the origin of the dependence of high harmonic yield on the ellipticity, which is studied in detail in Chapter 5.

#### 4.5.2 Isolated Attosecond Pulse Generation

#### 4.5.2.1 Principle of the Polarization Gating

The polarization gating is based on the strong dependence of the attosecond pulse generation efficiency on the ellipticity of the near infrared

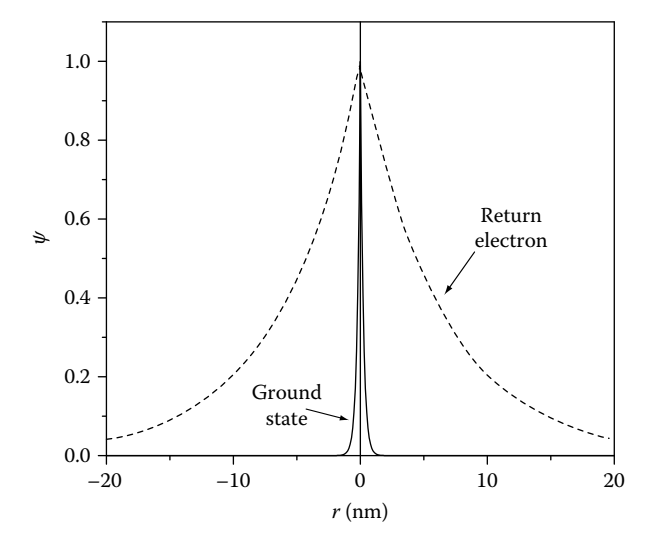


Figure 4.39 Quantum diffusion in linearly polarized field.

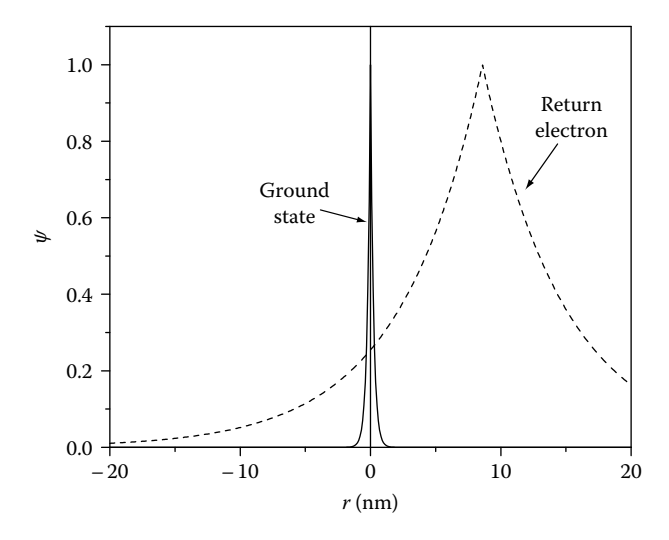


Figure 4.40 Quantum diffusion in circularly polarized field.

laser,  $\xi$ . To create a temporal gate, the polarization state of a laser pulse changes from circular to linear and back to circular again. As a result, the electron freed by the laser field will be driven away from the parent ion at both the head and tail parts of the laser pulse by the transverse component of the field. This will eliminate the possibility of recombination of the electron with the parent ion. Thus, attosecond pulses can only be produced by the center portion of the laser pulse that is nearly linearly polarized. This linearly polarized portion is where the gate opens and it could be much shorter than the input pulse duration. The gate width should be narrower than the spacing between adjacent attosecond pulses, 1.3 fs, for Ti:Sapphire lasers to generate singly isolated attosecond pulses.

We can draw an analogy between the polarization gating for generating single isolated attosecond pulses and the Pockels cell pulse picker in femtosecond lasers. In both cases, a single pulse is extracted from a pulse train. Interestingly, the attosecond polarization gating occurs during the generation process. In other words, all the pulses in the train except one are aborted before they are born.

#### 4.5.2.2 Laser Field

The laser field with a time-dependent ellipticity for polarization gating can be generated by the superposition of a left and a right-circularly polarized Gaussian pulse, as illustrated in Figure 4.41, which was suggested by Platonenko and Strelkov in 1999. The advantage of this scheme is that laser pulses with only one center frequency are required, which is easy to implement experimentally.

For a circularly polarized pulse,  $E_{x0} = E_{y0} = E_0$ , where  $E_{x0}$ ,  $E_{y0}$ , and  $E_0$  are the peak field amplitude components and the total amplitude. We consider the case where  $E_0$ , carrier frequency  $\omega_0$ , pulse duration  $\tau_p$ , and carrier-envelope phase  $\varphi_{CE}$  are the same for the two counter-rotating pulses. The delay between them,  $T_d$ , is assumed to be an integral number, n, of optical periods for simplifying the analysis. In principle,  $T_d$  can take any value. The FWHM of the spectrum of each circularly polarized is  $\Delta\omega = 4\ln 2/\tau_p$ .

The electric fields of the left and right circularly polarized pulses propagating in the z direction are

$$\vec{\varepsilon}_{l}(t) = E_{0}e^{-2\ln(2)\left(\frac{t-T_{d}/2}{\tau_{p}}\right)^{2}} \times \left[\hat{i}\cos(\omega_{0}t + \varphi_{CE}) + \hat{j}\sin(\omega t + \varphi_{CE})\right](-1)^{n}, \quad (4.136)$$

and

$$\vec{\varepsilon}_r(t) = E_0 e^{-2\ln(2)\left(\frac{t+T_d/2}{\tau_p}\right)^2} \times \left[\hat{i}\cos(\omega_0 t + \varphi_{CE}) - \hat{j}\sin(\omega_0 t + \varphi_{CE})\right] (-1)^n. \tag{4.137}$$

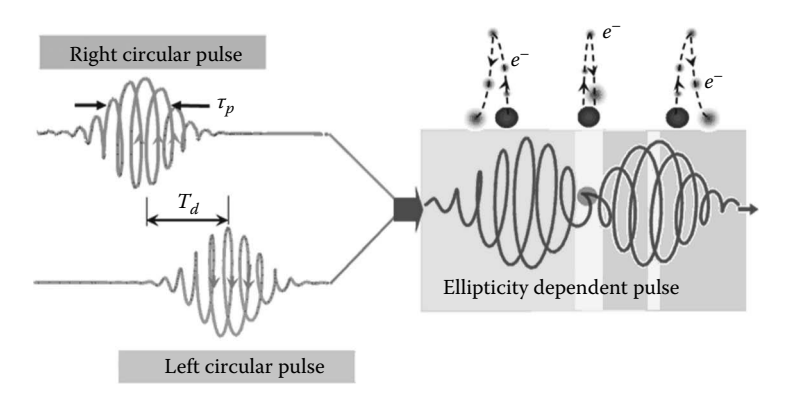


**Figure 4.41** Creation of laser pulse for polarization gating. (Reprinted from Shan, B. et al., *J. Mod. Opt.*, 52, 277, 2005.)

The total field can be resolved into two orthogonally polarized components. They are named as driving and gating field, respectively, because of the functions they serve. The driving field polarized in x direction generates the attosecond pulse, whereas the gating field in the y direction suppresses the attosecond emission outside of the polarization gate.

The driving field can be expressed as

$$\varepsilon_{drive}(t) = E_0 \left[ e^{-2\ln 2\frac{(t+T_d/2)^2}{\tau_p^2}} + e^{-2\ln 2\frac{(t-T_d/2)^2}{\tau_p^2}} \right] \cos(\omega_0 t + \varphi_{CE}). \quad (4.138)$$

and the gating field is

$$\varepsilon_{gate}(t) = E_0 \left[ e^{-2\ln 2^{\frac{(t+T_d/2)^2}{\tau_p^2}}} - e^{-2\ln 2^{\frac{(t-T_d/2)^2}{\tau_p^2}}} \right] \sin(\omega_0 t + \varphi_{CE}), \quad (4.139)$$

In the frequency domain, the driving and gating pulses are

$$\tilde{E}_{drive}(\omega) = E_0 e^{-\left(\frac{\omega - \omega_0}{\Delta \omega}\right)^2} \frac{1}{2} \left( e^{-i(\omega - \omega_0)\frac{T_d}{2}} + e^{i(\omega - \omega_0)\frac{T_d}{2}} \right) e^{i(\omega - \omega_0)\frac{T_d}{2}}$$

$$= E_0 e^{-\left(\frac{\omega - \omega_0}{\Delta \omega}\right)^2} \cos\left((\omega - \omega_0)\frac{T_d}{2}\right) e^{i(\omega - \omega_0)\frac{T_d}{2}}, \tag{4.140}$$

and

$$\tilde{E}_{gate}(\omega) = E_0 e^{-\left(\frac{\omega - \omega_0}{\Delta \omega}\right)^2} \frac{1}{2} \left( e^{-i(\omega - \omega_0)\frac{T_d}{2}} - e^{i(\omega - \omega_0)\frac{T_d}{2}} \right) e^{i(\omega - \omega_0)\frac{T_d}{2}} e^{i\frac{\pi}{2}}$$

$$= E_0 e^{-\left(\frac{\omega - \omega_0}{\Delta \omega}\right)^2} \sin\left((\omega - \omega_0)\frac{T_d}{2}\right) e^{i\omega^{\frac{T_d}{2}}}.$$
(4.141)

The power spectra of these two fields are  $I_{drive}(\omega) = I_0 e^{-2(\omega - \omega_0/\Delta\omega)^2} \cos^2\left[(\omega - \omega_0)\frac{T_d}{2}\right]$  and  $I_{gate}(\omega) = I_0 e^{-2(\omega - \omega_0/\Delta\omega)^2} \sin^2\left[(\omega - \omega_0)\frac{T_d}{2}\right]$ , respectively. The peak intensity  $I_0$  and the peak field amplitude are related by  $I_0 = \epsilon_0 c E_0^2$ , which is different from that for the linearly different pulse where  $I_0 = 1/2\epsilon_0 c E_0^2$ . The spectra can be measured with a spectrometer. A polarizer can be used to select one of them before sending to the spectrometer. There is a dip at  $\omega = \omega_0$  for the gating field spectrum. The delay  $T_d$  can be determined from the spectrum modulation.

#### 4.5.2.3 Fields inside the Polarization Gate

A parameter  $\gamma$  can be introduced to describe the delay between the two circular pulses such that

$$T_d = \gamma \tau_p. \tag{4.142}$$

The driving and gating fields can be rewritten as

$$\varepsilon_{drive}(t) = E_0 A_{drive}(t) \cos(\omega_0 t + \varphi_{CE}). \tag{4.143}$$

and

$$\varepsilon_{gate}(t) = E_0 A_{gate} \sin(\omega_0 t + \varphi_{CE}). \tag{4.144}$$

While the envelope of the driving and gating fields are

$$A_{drive}(t) = e^{-2\ln 2\left(\frac{t}{\tau_p} + \frac{\gamma}{2}\right)^2} + e^{-2\ln 2\left(\frac{t}{\tau_p} - \frac{\gamma}{2}\right)^2},$$
 (4.145)

and

$$A_{gate}(t) = e^{-2\ln 2\left(\frac{t}{\tau_p} + \frac{\gamma}{2}\right)^2} - e^{-2\ln 2\left(\frac{t}{\tau_p} - \frac{\gamma}{2}\right)^2}.$$
 (4.146)

For mathematical simplicity, we consider the case that the driving field is a constant at the center of the polarization gate. This requires

$$\frac{d^2}{dt^2} A_{drive}(t) \Big|_{t=0} = 0. {(4.147)}$$

Since

$$-\frac{\tau_{p}}{4 \ln 2} \frac{d}{dt} A_{drive}(t) = e^{-2 \ln 2 \left(\frac{t}{\tau_{p}} + \frac{\gamma}{2}\right)^{2}} \left(\frac{t}{\tau_{p}} + \frac{\gamma}{2}\right) + e^{-2 \ln 2 \left(\frac{t}{\tau_{p}} - \frac{\gamma}{2}\right)^{2}} \left(\frac{t}{\tau_{p}} - \frac{\gamma}{2}\right), \tag{4.148}$$

we can assume

$$-\frac{\tau_p^2}{4\ln 2} \frac{d^2}{dt^2} A_{drive}(t) = e^{-2\ln 2\left(\frac{t}{\tau_p} + \frac{\gamma}{2}\right)^2} \left[ 1 - 4\ln 2\left(\frac{t}{\tau_p} + \frac{\gamma}{2}\right)^2 \right] + e^{-2\ln 2\left(\frac{t}{\tau_p} - \frac{\gamma}{2}\right)^2} \left[ 1 - 4\ln 2\left(\frac{t}{\tau_p} - \frac{\gamma}{2}\right)^2 \right], \quad (4.149)$$

which leads to

$$\gamma = \frac{1}{\sqrt{\ln 2}} \approx 1.2. \tag{4.150}$$

This corresponds to the case where the delay is not much longer than the pulse duration.

In the range  $-1/2\tau_p < t < -1/2\tau_p$ , the envelope function of the driving field can be expressed approximately by

$$A_{drive}(t) = \frac{2}{\sqrt{e}} \approx 1.213,$$
 (4.151)

In the same time range,  $A_{\it gate}$  (t) is close to a linear function. The slope is

$$-\frac{\tau_{p}}{4 \ln 2} \frac{d}{dt} A_{gate}(t) = e^{-2 \ln 2 \left(\frac{t}{\tau_{p}} + \frac{\gamma}{2}\right)^{2}} \left(\frac{t}{\tau_{p}} + \frac{\gamma}{2}\right)$$
$$-e^{-2 \ln 2 \left(\frac{t}{\tau_{p}} - \frac{\gamma}{2}\right)^{2}} \left(\frac{t}{\tau_{p}} - \frac{\gamma}{2}\right). \tag{4.152}$$

At t = 0 this becomes

$$\frac{d}{dt}A_{gate}(t)|_{t=0} = 4\sqrt{\frac{\ln 2}{e}} \frac{1}{\tau_p}.$$
 (4.153)

Thus,

$$A_{gate}(t) = 4\sqrt{\frac{\ln 2}{e}} \frac{t}{\tau_p} \approx 2\frac{t}{\tau_p}.$$
 (4.154)

The two field components are

$$E_{drive}(t) = \frac{2}{\sqrt{e}} E_0 \cos(\omega_0 t + \varphi_{CE}), \qquad (4.155)$$

and

$$E_{gate}(t) = 4\sqrt{\frac{\ln 2}{e}}E_0 \frac{t}{\tau_p} \sin(\omega_0 t + \varphi_{CE}). \tag{4.156}$$

## 4.5.2.4 Electron Trajectories

We consider the case that  $\tau_p = 2T_0$ . The time range  $-1/2\tau_p < t < +1/2\tau_p$  can also be expressed in terms of optical cycles, i.e.,  $-T_0 < t < +T_0$ . The trajectories that correspond to the maximum returning kinetic energy are analyzed.

For  $\varphi_{CE} = 0$ , there are two short trajectories that electrons are released and returned within the time range. We consider the trajectory in the *x* and *y* directions separately. The two field components are

$$\varepsilon_{drive}(t) = E_{d0}\cos(\omega_0 t) \tag{4.157}$$

and

$$\varepsilon_{gate}(t) = E_{g0} \frac{t}{\tau_p} \sin(\omega_0 t), \qquad (4.158)$$

where 
$$E_{d0} = \left(\frac{2}{\sqrt{e}}\right) E_0, E_{g0} = 4\sqrt{\ln 2/e} E_0.$$

In the *x* direction, the motion is the same as that in a linearly polarized monochromatic field.

$$\frac{x(t)}{x_d} = \frac{1}{2} \left[ \cos(\omega_0 t) - \cos(\omega_0 t') \right] + \sin(\omega_0 t') \omega_0 (t - t'). \tag{4.159}$$

Here,  $x_d = 2eE_{d0}/m\omega_0^2$ , t' is the electron's birth time. The returning energy is the maximum for the electron released at  $\omega_0 t' = 0.05 \times 2\pi$  rad and returns at  $\omega_0 t = 0.7 \times 2\pi$ .

In the y direction, the equation of motion is

$$m\frac{d^2y}{dt^2} = -eE_{g0}\frac{t}{\tau_p}\sin(\omega_0 t).$$
 (4.160)

And the velocity is

$$\frac{m\omega_0^2}{eE_{g0}} \frac{dy}{dt}$$

$$= \frac{1}{\tau_p} \left[ \omega_0 t \cdot \cos(\omega_0 t) - \sin(\omega_0 t) + \sin(\omega_0 t') - \omega_0 t' \cdot \cos(\omega_0 t') \right].$$
(4.161)

The displacement then becomes

$$\frac{m\omega_0^3}{eE_{g0}}\tau_p y = 2[\cos(\omega_0 t) - \cos(\omega_0 t')] + \omega_0 t \cdot \sin(\omega_0 t) - \omega_0 t'$$

$$\cdot \sin(\omega_0 t') + [\sin(\omega_0 t') - \omega_0 t' \cdot \cos(\omega_0 t')]\omega_0 (t - t'). \quad (4.162)$$

For  $\omega_0 t' = 0.05 \times 2\pi$  rad and  $\omega_0 t = 0.7 \times 2\pi$ , the right hand side of equation numerically becomes -6.758. Thus the transverse displacement is

$$y_c = -\frac{6.758}{2\pi} \frac{T_0}{\tau_p} \frac{eE_{g0}}{m\omega_0^2} \approx -1.08 \frac{T_0}{\tau_p} \frac{eE_{g0}}{m\omega_0^2}.$$
 (4.163)

The typical Ti:Sapphire laser intensity for attosecond pulse generation is  $5 \times 10^{14} \text{ W/cm}^2$ ,  $y_0 \approx 1 \text{ nm}$ .

#### 4.5.2.5 Polarization Gate Width

The electric field of the NIR laser pulse for polarization gating can be expressed as

$$\vec{\varepsilon}(t) = \varepsilon_{drive}(t)\hat{i} + \varepsilon_{gate}(t)\hat{j}. \tag{4.164}$$

The time-dependent ellipticity is

$$\xi(t) = \frac{A_{gate}(t)}{A_{drive}(t)} = \frac{\left| e^{-2\ln(2)\left(\frac{t-T_d/2}{\tau_p}\right)^2} - e^{-2\ln(2)\left(\frac{t+T_d/2}{\tau_p}\right)^2} \right|}{\left[ e^{-2\ln(2)\left(\frac{t-T_d/2}{\tau_p}\right)^2} + e^{-2\ln(2)\left(\frac{t+T_d/2}{\tau_p}\right)^2} \right]}$$

$$= \frac{\left| 1 - e^{-4\ln(2)\frac{T_d}{\tau_p^2}t} \right|}{1 + e^{-4\ln(2)\frac{T_d}{\tau_p^2}t}}, \tag{4.165}$$

Figure 4.42 shows the variation of the ellipticity inside the laser pulse using Equation 4.165 when  $\tau_p = 8$  fs long and  $T_d = 15$  fs.

For harmonic orders higher than the 21st, the harmonic signal drops by more than an order of magnitude when the ellipticity increases from 0 to 0.2. Therefore, the attosecond pulse is generated in the temporal range around t=0 and  $\xi \leq 0.2$ , where the ellipticity decreases almost linearly with |t| in the center portion,

$$\xi(t) \approx \left| 2\ln(2) \frac{T_d}{\tau_p^2} t \right|. \tag{4.166}$$

The time interval, where the ellipticity is less than a certain threshold value  $\xi_{th}$ , is thus

$$\delta t_G = \frac{\xi_{th}}{\ln{(2)}} \frac{\tau_p^2}{T_d}.$$
 (4.167)

It is named the polarization gate width. For harmonic order higher than 20, we can set  $\xi_{th} = 0.2$ . It suggests that there are two ways to reduce the

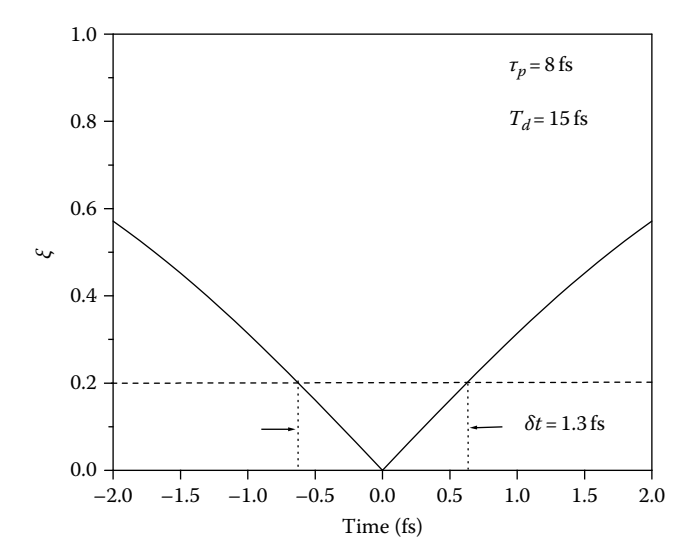


Figure 4.42 Time-dependent ellipticity and polarization gate width.

polarization gate width. The first one is to use shorter pulses; the second one is to increase the delay between the pulses. Reducing pulse width is more effective because of the quadratic dependence.

The second approach is at the cost of losing laser field strength for a given laser-pulse energy. The amplitude of the linear field for a given delay and pulse duration can be calculated from Equation 4.164 at t = 0,

$$E(0) = 2E_0 e^{-\frac{\ln(2)}{2} \left(\frac{T_d}{\tau_p}\right)^2}. (4.168)$$

The field is significantly lower than the peak field of each pulse,  $E_0$ , for  $T_d \gg \tau_p$ , which means that the field outside the gate is much stronger than the inside one. In such case, the conversion efficiency is low because most of the laser energy is outside the gate.

In experiments, one should choose  $T_d \approx \tau_p$  and  $\delta t_G = T_0/2$ . In this case,  $\tau_p = \delta t_G/0.3 = T_0/0.6$ . For Ti:Sapphire laser,  $\tau_p = 2.67$  fs/0.6 = 4.45 fs. The field amplitude inside the gate,  $E(0) = \sqrt{2}E_0$ , which is higher than the outside. The gate width

$$\delta t_G = 0.3\tau_p. \tag{4.169}$$

Equation 4.169 indicates that applying polarization gating to high harmonic generation is equivalent to the reduction of the duration of a linearly polarized pulse by a factor of three. When  $\delta t_G = T_0/2$ , it is expected that only a single attosecond pulse is produced in the plateau region of the XUV spectrum. The calculated required delay time  $T_d$  for producing a single isolated pulse as a function of the laser-pulse duration is shown in Figure 4.43.

## 4.5.2.6 Optics for Creating Laser Pulse for Polarization Gating

Laser field with the required time-dependent ellipticity can be constructed by a simple method illustrated in Figure 4.44. The first quartz plate is a

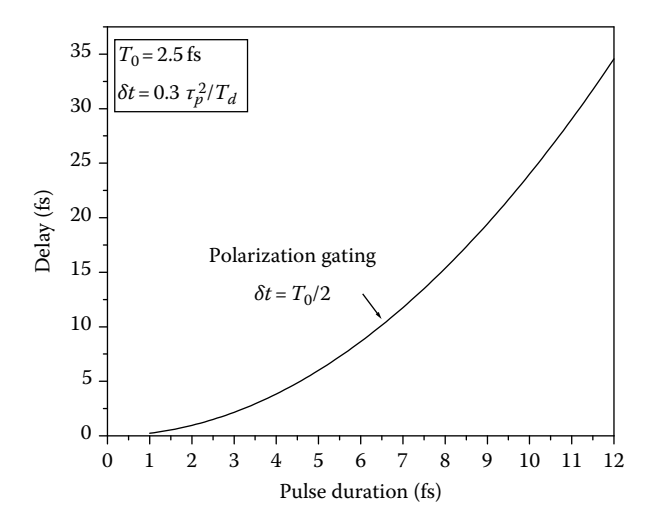


**Figure 4.43** The required delay between two counter-rotating circularly polarized pulses for extracting a single isolated attosecond pulse from a pulse train. The gate width equals to one half of an optical cycle.

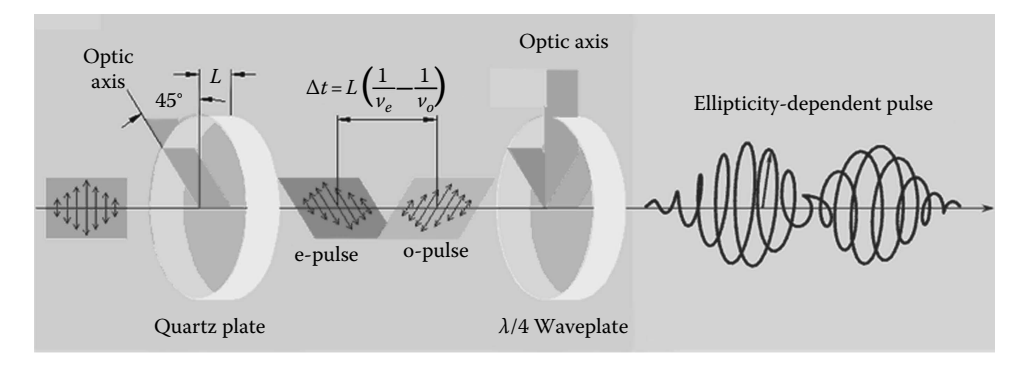


**Figure 4.44** Time-dependent ellipticity and polarization gate width. (Reprinted from Shan, B. et al., *J. Mod. Opt.*, 52, 277, 2005.)

multiple order whole-wave plate where the linearly polarized input pulse is evenly divided into an o-ray and an e-ray by setting its optic axis  $45^{\circ}$  with respect to the input polarization. The o-pulse and the e-pulse are separated in time because the o-pulse and e-pulse travelled at different group velocities,  $v_o$  and  $v_e$ . The delay is proportional to the plate thickness, L. The durations of the two pulses are almost the same because the difference of the group velocity dispersions is small for the two polarization orientations. An achromatic quarter-wave plate is placed with its optic axis along the initial input polarization ( $45^{\circ}$  to o-pulse and e-pulse). It can convert broadband o-pulse and e-pulse into left- and right-circularly polarized light. The superposition of these two pulses produced a pulse whose ellipticity changes rapidly with time. The dispersion introduced by these two components can be compensated by chirped mirrors.

#### 4.5.2.7 Upper Limit of Laser-Pulse Duration

Although the gate width of polarization gating can be set to half a laser cycle with very long laser pulse as long as the delay between the two circularly polarized pulses is large enough, it is just one of the necessary conditions for generating isolated attosecond pulses. Another necessary condition is that the ground-state population of the atom responsible for the attosecond light emission inside the polarization gate cannot be zero. Otherwise, there will be no atom emits XUV light. In other words, the ionization of the target atom by the laser field before the polarization gate should not completely deplete the ground-state population. The ionization probability of argon atom as a function of the laser-pulse duration is shown in Figure 4.45. The calculations are done with the ADK rate and the gate width is kept as half of a laser cycle. The pulse duration at which the ground state is almost completely depleted is  $\sim$ 7 fs, which is upper limit for argon atom.

Figure 4.46 shows the ionization probabilities of the Helium atom within the NIR laser pulse for gating. The initial pulse durations are 5 and 10 fs, respectively. The laser intensities are the same for both pulses at time t=0 fs. The attosecond pulses are generated by electrons freed at the time interval between the two dashed lines. The ionization probability at t=0 is 93.4% for the 10 fs pulses. We can conclude that pulses less than 10 fs should be used for generating isolated attosecond pulse with Helium atoms.

# 4.6 Summary

The semiclassical model is intuitive and easy to use. However, the amplitude information of the attosecond pulses is lost in the calculations. The quantum theory discussed in Chapter 5 allows the calculation of both the amplitude and phase of the attosecond radiation, and is more powerful.

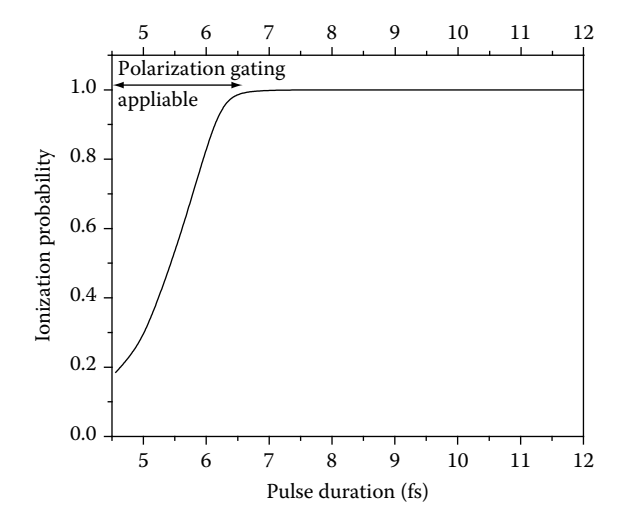
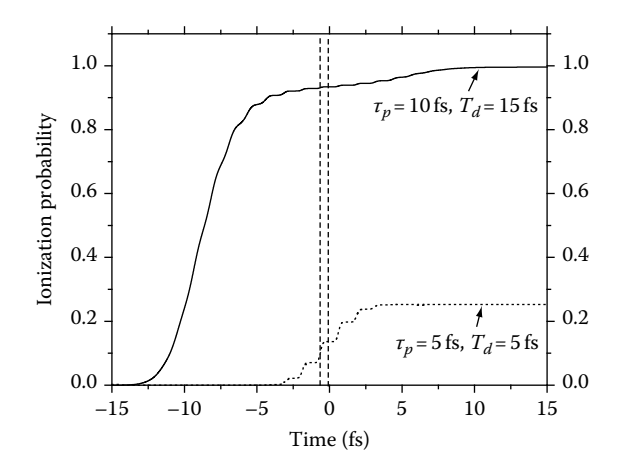


Figure 4.45 Ionization probability of the atom in the ground state.



**Figure 4.46** The ionization probabilities of a helium atom in laser fields with a time dependent ellipticity. The laser pulse is formed by the combination of a left-hand circularly polarized pulse and a right-hand circularly polarized pulse. Solid line: both circular pulses are 10 fs and the delay between them is 15 fs. The dotted line is obtained when the pulse duration is 5 fs and the delay is 5 fs. The intensity at t=0 is  $1.4\times10^{15}$  W/cm². The carrier-envelope phase of the laser pulse is  $\pi/2$  rad. The high harmonics are generated within the time interval between the two dashed lines. (From Z. Chang, *Phys. Rev. A*, 71, 023813, 2005. Copyright 2005 by the American Physical Society.)

## **Problems**

- **4.1** Plot the maximum electron displacement  $x_0$  in the intensity range of  $1 \times 10^{14}$  to  $1 \times 10^{15}$  W/cm<sup>2</sup> for lasers centered at 0.8 and 1.6  $\mu$ m.
- **4.2** Plot the ponderomotive energy in the intensity range of  $1 \times 10^{14}$  to  $1 \times 10^{15}$  W/cm<sup>2</sup> for lasers centered at 0.8 and 1.6  $\mu$ m.
- **4.3** Plot trajectories for two electrons, one ionized at  $\omega_0 t' = \pi/4$  and another at  $\omega_0 t' = \pi/2$ . The laser period is 2.67 fs and the intensity is  $1 \times 10^{15}$  W/cm<sup>2</sup>. Find the time that the electrons return to the parent ion for the first time.
- **4.4** Find the return time for the two electrons in Problem 4.3. Compare the results with the findings in Problem 4.3.
- **4.5** Plot the return time span for the laser wavelength range of 400–2000 nm.
- **4.6** Plot the return time spans of the long and short trajectory for the laser wavelength range of 400–2000 nm.
- **4.7** Calculate the chirp of the short trajectory at two intensities,  $1 \times 10^{14}$  and  $1 \times 10^{15}$  W/cm<sup>2</sup> for lasers centered at 0.8 and 1.6  $\mu$ m. Use the as/eV unit.
- **4.8** Calculate the Keldysh parameter when Xe atoms are placed in a Ti: Sapphire laser field with  $1 \times 10^{14}$  W/cm<sup>2</sup>. Compare that with He atoms in the same laser field.
- **4.9** Calculate the electron tunneling times and the electron velocities in the barrier in Problem 4.8.
- **4.10** For l = 1, prove that the PPT rate for m = 0 is larger than those for  $m = \pm 1$ . (*Hint:* compare  $G_{lm}$ .)

- **4.11** Calculate and plot the ionization rate of an argon atom by laser centered at 790 nm in the intensity range of  $3 \times 10^{13}$  to  $3.5 \times 10^{14}$  W/cm<sup>2</sup>. Compare the magnitude of the rate with that of helium shown in Figure 4.10.
- **4.12** Plot the electron trajectory in a two-color laser field.
- **4.13** Plot the return time in a two-color laser field.
- **4.14** Plot the returning energy in a two-color laser field.
- **4.15** Plot the return time for  $\alpha = 0$ , 0.1, and 0.2 The relative phases  $\phi_{12} = 0$ .
- **4.16** For  $F_a/F_0 = 0.01$ , calculate the ratio between the cycle averaged ionization rate and the ADK rate.
- **4.17** Calculate the ionization probability of Ar atom with linearly polarized 20 fs lasers at  $1 \times 10^{14}$  W/cm<sup>2</sup>. Compare that with 200 fs lasers at the same intensity. Explain the reason the probability depends on the pulse duration.
- **4.18** Calculate the saturation intensity of argon atoms with linearly polarized 20 fs lasers. Compare that with 200 fs lasers. Explain the reason the saturation intensity depends on the pulse duration.
- **4.19** Calculate the saturation intensity of argon and neon atoms with linearly polarized 20 fs lasers. Explain the reason the saturation intensity depends on the atomic species.
- **4.20** For a 7 fs laser centered at 750 nm, calculate the delay between the two counter-rotating circular pulse so that the polarization gate width is half of optical cycle.
- **4.21** When a quartz plate is used to obtain the delay in Problem 4.20 in Figure 4.44, calculate the thickness of the quartz plate.

#### References

# Ionization by Laser Field

- Agostini, P., F. Fabre, G. Mainfray, G. Petite, and N. K. Rahman, Free-free transitions following six-photon ionization of xenon atoms, *Phys. Rev. Lett.* **42**, 1127 (1979).
- Ammosov, M. V., N. B. Delone, and V. P. Krainov, Tunnel ionization of complex atoms and atomic ions in an alternating electromagnetic field, *Sov. Phys. JETP* 64, 1191 (1986).
- Chang, B., P. R. Bolton, and D. N. Fittinghoff, Closed-form solutions for the production of ions in the collisionless ionization of gases by intense lasers, *Phys. Rev. A* 47, 4193 (1993).
- DeWitt, M. J. and R. J. Levis, Calculating the Keldysh adiabaticity parameter for atomic, diatomic, and polyatomic molecules, J. Chem. Phys. 108, 7739 (1998).
- Faisal, F. H. M., Multiple absorption of laser photons by atoms, *J. Phys. B* **6**, L89 (1973).
- Ilkov, F. A. et al., Ionization of atoms in the tunnelling regime with experimental evidence using Hg atoms, *J. Phys. B At. Mol. Opt. Phys.* **25**, 4005 (1992).
- Keldysh, L. V., Ionization in the field of a strong electromagnetic wave, *Sov. Phys. JETP* 20, 1307 (1965); *Zh. Eksp.Teor. Fiz.* 47, 1945 (1964).
- Larochelle, S. F. J., A. Talebpour, and S. L. Chin, Coulomb effect in multiphoton ionization of rare-gas atoms, J. Phys. B At. Mol. Opt. Phys. 31, 1215 (1998).
- Mainfray, G. and G. Manus, Multiphoton ionization of atoms, Rep. Prog. Phys. 54, 1333 (1991).
- Mishima, K., M. Hayashi, J. Yi, S. H. Lin, H. L. Selzle, and E. W. Schlag, Generalization of Keldysh's theory, *Phys. Rev. A* **66**, 033401 (2002).

- Nagaya, K., K. Mishima, M. Hayashi, and S. H. Lin, Compact photo-ionization rate based on Keldysh theory, J. Phys. Soc. Japan 75, 044302 (2006).
- Perelomov, M. and V. S. Popov, Ionization of atoms in alternating electric field. III, Sov. Phys. JETP 25, 336 (1967).
- Perelomov, M., V. S. Popov, and M. V. Terent'ev, Ionization of atoms in alternating electric field, *Sov. Phys. JETP* **23**, 924 (1966).
- Scrinzi, A., M. Geissler, and T. Brabec, Ionization above the Coulomb barrier, *Phys. Rev. Lett.* **83**, 706 (1999).
- Trombetta, F., S. Basile, and G. Ferrante, Multiphoton-ionization transition amplitudes and the Keldysh approximation, *Phys. Rev. A* **40**, 2774 (1989); *Phys. Rev. A* **41**, 4096 (1990).
- van der Hart, H. W., B. J. S. Doherty, J. S. Parker, and K. T. Taylor, Benchmark multiphoton ionization rates for He at 390 nm, *J. Phys. B At. Mol. Opt. Phys.* **38**, L207 (2005).

## Three-Step Model

- Corkum, P. B., Plasma perspective on strong-field multiphoton ionization, *Phys. Rev. Lett.* 71, 1994 (1993).
- Corkum, P. B. and Z. Chang, The attosecond revolution, Opt. Photon. News 19, 24 (2008).
- Kulander, K. C., K. J. Schafer, and J. L. Krause, Super-Intense Laser-Atom Physics, NATO ASI, Ser. B, Vol. 316, p. 95, Plenum, New York (1993).

## Cutoff of High Harmonic Generation

- Chang, Z., A. Rundquist, H. Wang, H. Kapteyn, and M. Murnane, Generation of coherent soft x-rays at 2.7 nm using high harmonics, *Phys. Rev. Lett.* **79**, 2967 (1997).
- Popmintchev, T., M.-C. Chen, O. Cohen, M. E. Grisham, J. J. Rocca, M. M. Murnane, H. C. Kapteyn, Extended phase matching of high harmonics driven by midinfrared light, *Opt. Lett.* 33, 2128 (2008).
- Seres, J., E. Seres, A. J. Verhoef, G. Tempea, C. Streli, P. Wobrauschek, V. Yakovlev, A. Scrinzi, C. Spielmann, and F. Krausz, Laser technology: Source of coherent kiloelectronvolt x-rays, *Nature* 433, 596 (2005).
- Shan, B. and Z. Chang, Dramatic extension of the high-order harmonic cutoff by using a long-wavelength pump, *Phys. Rev. A* **65**, 011804(R) (2001).
- Spielmann, Ch., N.H. Burnett, S. Sartania, R. Koppitsch, M. Schnürer, C. Kan, M. Lenzner, P. Wobrauschek, and F. Krausz, Generation of coherent X-rays in the water window using 5-femtosecond laser pulses, *Science* 278, 661 (1997).
- Takahashi, E. J., T. Kanai, K. L. Ishikawa, Y. Nabekawa, and K. Midorikawa, Coherent water window x ray by phase-matched high-order harmonic generation in neutral media, *Phys. Rev. Lett.* **101**, 253901 (2008).
- Xiong, H., H. Xu, Y. Fu, J. Yao, B. Zeng, W. Chu, Y. Cheng, Z. Xu, E. J. Takahashi, K. Midorikawa, X. Liu, and J. Chen, Generation of a coherent x ray in the water window region at 1 kHz repetition rate using a mid-infrared pump source, *Opt. Lett.* 34, 1747 (2009).

# Two-Color Gating

- Oishi, Y., M. Kaku, A. Suda, F. Kannari, and K. Midorikawa, Generation of extreme ultraviolet continuum radiation driven by a sub-10-fs two-color field, *Opt. Express* 14, 7230 (2006).
- Pfeifer, T., L. Gallmann, M. J. Abel, D. M. Neumark, and S. R. Leone, Single attosecond pulse generation in the multicycle-driver regime by adding a weak second-harmonic field, *Opt. Lett.* 31, 975 (2006).

# Polarization Gating

- Chang, Z., Single attosecond pulse and xuv supercontinuum in the high-order harmonic plateau, *Phys. Rev. A* **70**, 043802 (2004).
- Chang, Z., Chirp of the attosecond pulses generated by a polarization gating, *Phys. Rev.* A 71, 023813 (2005).

- Corkum, P. B., N. H. Burnett, and M. Y. Ivanov, Subfemtosecond pulses, *Opt. Lett.* 19, 1870 (1994).
- Kazamias, S. and Ph. Balcou, Intrinsic chirp of attosecond pulses: Single-atom model versus experiment, *Phys. Rev. A* **69**, 063416 (2004).
- Platonenko, V. T. and V. V. Strelkov, Single attosecond soft-x-ray pulse generated with a limited laser beam, *J. Opt. Soc. Am. B* **16**, 435 (1999).
- Shan, B., S. Ghimire, and Z. Chang, Generation of attosocond XUV supercontinuum by polarization gating, *J. Mod. Opt.* **52**, 277 (2005).